AIChE

Spectral Characterization of Static Mixers. The S-Shaped Micromixer as a Case Study

F. Garofalo, A. Adrover, S. Cerbelli, and M. Giona
Dipt. di Ingegneria Chimica, Università di Roma ''La Sapienza'', Via Eudossiana 18, 00184 Roma, Italy

DOI 10.1002/aic.11994
Published online October 1, 2009 in Wiley InterScience (www.interscience.wiley.com).

We investigate the steady-state performance of a planar micromixer composed of several S-shaped units. Mixing efficiency is quantified by the decay of the scalar variance downstream the device for generic feeding conditions. We discuss how this decay is controlled by the spectral properties of the advection-diffusion Floquet operator, $\mathcal{F}$, that maps a generic scalar profile at the inlet of a single unit into the corresponding profile at the unit outlet section. Two advantages characterize the Floquet operator approach —(i) it allows to analyze an arbitrarily long device and (ii) it provides a quantitative assessment of mixing efficiency that is independent of the feeding conditions and that depends solely on the interaction between advection and diffusion.
 AIChE J, 56: 318–335, 2010
Keywords: motionless micromixer, helical flow, advection-diffusion equation, mixing, homogenization exponent, spectral analysis

Motivation and Background

Fluid mixing by chaotic advection has attracted considerable attention in the past 25 years as an efficient route to homogenize segregated mixtures in the low Reynolds number regime (see, e.g., Aref [1], and therein cited references for a historical perspective on the subject). Up to the last decade, the practical implications of the swiftly growing background of knowledge in this research field had been confined to specific processes where turbulence is either unattainable or undesirable, such as those involving highly viscous fluids (e.g., polymers) or shear-sensitive materials (e.g., cell suspensions), respectively.

In the past few years, the significant advances offered by microfabrication techniques have made it possible to construct continuous mixers and reactors whose characteristic cross sectional dimension can be of the order of few microns.[2] The advantages of implementing continuous processes at such small lengthscales can hardly be overestimated, as microflow devices open up new perspectives and unprecedented applications in both physicochemical[3] and life sciences.[2] Because of the small dimensions of the channels cross section, the vast majority of microflow devices operates in the laminar or even Stokes regime.[4] Besides, the domain of application of these devices, which often involves processing of biomolecules characterized by extremely low values of molecular diffusivity, makes it impractical to rely exclusively on molecular diffusion as a mixing mechanisms. Quantitatively, the necessity of exploiting convective mechanisms to enhance the mixing rate can readily be appreciated as soon as one considers that while the typical Re number of microflows ranges in the interval $10^{-2} \div 10^{2}$, the Pe number, yielding the ratio between a characteristic time for diffusion to that of convection, can reach values up to $Pe = 10^{6}$ when liquid mixtures are to be dealt with.[4]

For this reason, strategies that exploit a constructive interaction between advection and diffusion constitute a theoretical cornerstone for a rational development of microflow devices. In this respect, chaotic advection appears as a feasible alternative to turbulence, and it is therefore no surprise that the research on laminar mixing has been experiencing a second burst of activity since microflow devices made their first appearance.

In general terms, chaotic advection in open flow systems is generated by a secondary (cross sectional) flow that stretches and reorients the material interface between

Correspondence concerning this article should be addressed to M. Giona at max@giona.ing.uniroma1.it

segregated streams while they are being carried by the primary (axial) flow through the inflow-outflow device. The stretching and folding of the material interface has a twofold effect on the molecular mixing mechanism, namely, an increased interfacial area available for scalar transport and the amplification of scalar gradients in a direction transverse to the interface, which enhances the local Fickian flux. The simultaneous presence of these two phenomena can be regarded as the Lagrangian counterpart of the Eulerian incompressibility constraint associated with the velocity field.

As regards micromixers, depending on the process requirements and constraints, the secondary flow can be generated by using two conceptually different strategies, which define the classes of active and passive micromixers.[4]

The first (active micromixers) exploits the coupling between momentum transport and other physical phenomena, such as electric and magnetic fields (electrokinetic and magnetohydrodynamic mixers[4]). It is worth observing that this coupling is made possible by the small dimensions of the channels, so that scaling up active micromixers is typically impractical.

In passive micromixers, the secondary flow can be generated either by a complex design of the channel boundaries or, alternatively, by creating operating conditions that trigger the action of the nonlinear term in the momentum transport equation, which destroys the unidirectional character of the flow. An example of the first category of passive devices is the so-called split-and-recombine micromixer,[5,6] where the originally segregated streams entering the device are repeatedly divided and merged by the system boundary geometry. As in this type of mixers interface stretching and lamellar shrinking is imposed by the geometric structure of the boundaries, their design is typically optimized by considering creeping flow (Stokes) conditions. Despite their efficiency, these devices are typically associated with high pressure drops and nontrivial constructing issues.[7]

As an alternative, the secondary flow can be generated in much simpler geometries, such as curved pipes[8] or channels with square cross section,[9] by enforcing operating conditions that turn on the nonlinear character of Navier-Stokes equation while still maintaining the system in the laminar (steady state) flow regime. Thus, the working regimes of this type of devices imply much higher values of *Re* than those associated with micromixers based on a complex boundary geometry such as, e.g., the split-and-recombine mixer.

From a computational standpoint, the problem of assessing mixing efficiency associated with an advecting-diffusing scalar is challenging in that, at large values of the *Pe* number, numerical diffusion can overshadow molecular transport and compromise the validity of the numerical analysis.[5,6] This is particularly true whenever localized approaches such as finite differences, finite volumes, or finite elements are used. As this shortcoming is associated with all numerical simulations of advection-diffusion processes in the high *Pe* range, independently of both the scale (micro vs macro) and the nature (open vs closed) of the mixing domain, a number of strategies aimed at avoiding the direct solution of the Eulerian advection-diffusion equation have been proposed.[10,11] The crudest version of these approaches consists of analyzing only the convective aspect of mixing and assess mixing efficiency on the basis of purely kinematic (Lagrangian) indexes. Beyond Poincaré sections, which provide a global view of the trajectories in the mixing domain, relevant indexes that account for the local and global deformation process of the kinematic interface are stretch factor distributions, Lyapunov exponents, and topological entropy.[12,13] The kinematic approach has encountered a favorable response among researchers dealing with laminar mixing in micro-[14] and ordinary lengthscale motionless mixers[11] in view of numerical evidence that in globally chaotic conditions, a sensible estimate of mixing and reaction efficiency can be derived a posteriori by superimposing the action of diffusion (and, possibly, of chemical reactions) to the kinematic picture (see, e.g., Szalai et al.,[15] and therein cited references).

However, there are different shortcomings associated with a direct implementation of the kinematic approach to assess mixing performance of microflow devices, namely, (i) the typical *Pe* number falls in a range that is intermediate between that of a purely diffusive system (e.g., associated with a submicron scale device) and that associated with a convection-dominated process at ordinary lengthscales, (ii) the achievement of globally chaotic conditions, which in lab or industrial mixers can be accomplished through a careful design of baffles inserted within the channel,[11] is not constructively straightforward at these lengthscales, and (iii) in geometries of practical relevance, the interpolation of the discrete (CFD-computed) velocity field, and the numerical integration scheme for calculating flow trajectories can introduce spurious attractors that compromise the validity of the kinematic approach*.

All of these observations suggest that a direct solution of the advection diffusion equation, where the convection and diffusion processes act alongside each other simultaneously, is advisable when characterizing inflow–outflow microdevices. Also, global basis functions, such as Fourier modes, are better suited (whenever possible) for representing the finite-dimensional projection of the continuous model to be solved numerically.

The S-shaped cross-square duct (also referred to as serpentine channel or meander mixer), that we choose as case study in this article, can be considered as a benchmark test of passive micromixers in that it represents a good compromise between geometric simplicity and practical relevance.[14,16] It has been suggested that this geometric configuration might be the simplest architecture that can induce chaotic mixing,[14] provided that the *Re* number is large enough.

From a fluid dynamic standpoint, the characterization of the flow field in curved channels with square cross section has been object of several studies, which showed how a stable (i.e., discretization independent) solution up to relatively large values of the Dean number (order 500) can be obtained through standard CFD algorithms with reasonable computational effort (see next Section for details).

The numerical solution of the scalar transport equation is instead much more involved in view of the large values of the *Pe* number that are associated with liquid mixing. For instance, Vanka et al.[17] conducted a thorough numerical investigation of scalar mixing in a nonchaotic flow within a curved channel at $Re = 10$ up to $Pe = 10^5$ by using a finite difference scheme for the momentum and the diffusing scalar balance equations and reported that a mesh of 640×640 nodal points on the cross

*One of the most frequent occurrences of this phenomenon in inflow–outflow systems is constituted by fluid trajectories that collapse at a system boundary.

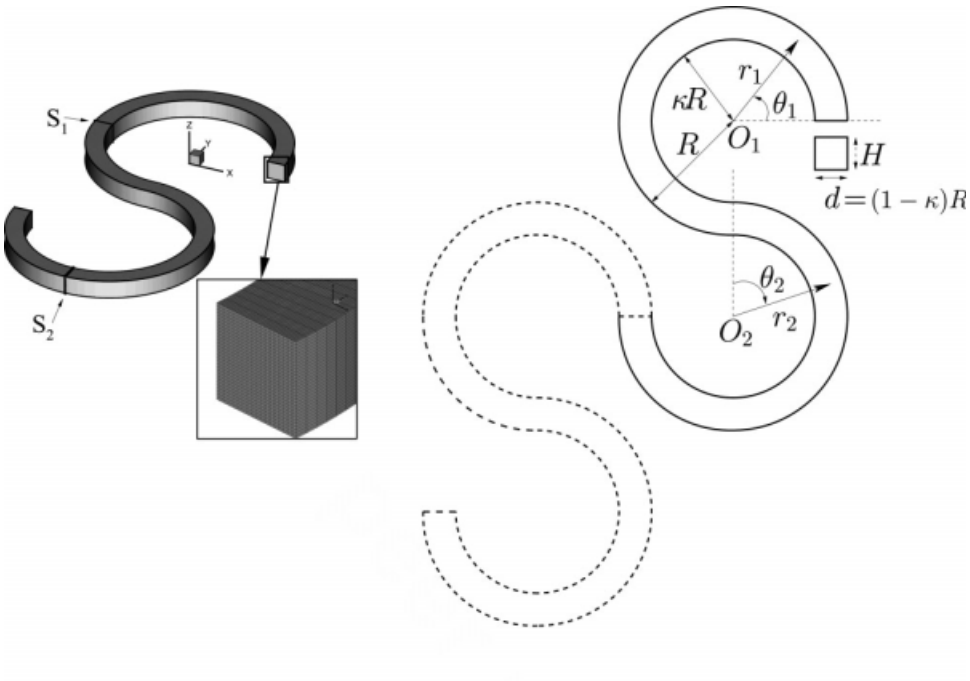

Figure 1. Left: Three-dimensional structure of the basic mixing unit. The zoomed-in region highlights the structure of the mesh used for the CFD solution of the flow field. Right: Definition of the geometric parameters and of the coordinate system.

section was needed for representing accurately the advection-diffusion process, whereas a much coarser grid (of order 32 × 32 nodes) was necessary for obtaining the same accuracy in the momentum transport equation.

Here, we use S-shaped prototype to illustrate a novel approach to the characterization of steady-state performance of inflow-outflow micromixers. This approach is based on the spectral properties (i.e., eigenvalues-eigenfunctions) of the input–output operator, which maps a generic scalar profile at the entrance of a single mixer element into the outlet profile at the the end of that element. The first few eigenvalues of the spectrum, ordered decreasingly with respect to their absolute value, provide a direct measure of the exponent governing the decay of the cross sectional scalar variance downstream the device axis.

We show that the spectral approach can yield a quantitative and objective characterization of mixing efficiency associated with a given velocity field and an assigned value of scalar diffusivity. Unlike other common measures of efficiency, such as, e.g., the mixing time,[18,19] this characterization is not specifically constrained to a particular choice of the inlet condition, provided that a sufficient number of eigenmodes are available to represent a generic inlet condition.

Statement of the Problem

System geometry and flow structure

The geometry of the S-shaped channel is represented in Figure 1. It is defined by two dimensionless parameters, namely, the ratio of the inner to the outer radius, κ and the ratio of the outer radius to the channel height $\alpha = R/H$. The total length of the unit is $L_u = 3\pi\overline{R}$, where the average radius $\overline{R}$ is given by $\overline{R} = (\kappa + 1)R/2$, whereas the cross sectional area is given by $S_c = R^2(1 - \kappa)/\alpha$. Throughout this article, we choose the values $\alpha = 5.5$ and $\kappa = 4.5/5.5 = 0.818181\ldots$ which represent a benchmark test case for which CFD data,[5] kinematic simulations,[5] and experimental results of passively diffusing tracers[14] are available in the Literature. We define a piecewise cylindrical coordinate system for each half unit of the mixer (denoted as r_1, θ_1, z and r_2, θ_2, z in the two halves of the first unit, see Figure 1) where the z variable is independent of the specific unit and is assumed directed upward the plane of the mixer. For each system half unit, we use cylindrical dimensionless variables, $\rho_n = r_n/R$ ($\kappa \le \rho_n \le 1$), θ_n ($0 \le \theta_n, \le 3\pi/2$) $n = 1, 2, \ldots$, and $\zeta_n = z/H$ ($0 \le \zeta_n \le 1$). Henceforth, the S-shaped curve through the center of each cross section, $\{\rho_n = (\kappa + 1)/2,\ 0 \le \theta_n \le 3\pi/2\}$ will be referred to as device axis (not to be confused with the axis of the cylindrical coordinate systems). Also, to identify a generic cross section in the n-th half unit downstream the device axis, we define a global azimuthal variable Θ, as

$$\Theta = \theta_n + \frac{3}{2}\pi(n-1), \tag{1}$$

and a dimensionless length N, given by

$$N = \frac{\Theta}{3\pi}, \tag{2}$$

which attains integer values at the end of each mixing unit.

The velocity field $\mathbf{v} = (v_\rho(\rho_n, \theta_n, \zeta_n), v_\theta(\rho_n, \theta_n, \zeta_n), v_\zeta(\rho_n, \theta_n, \zeta_n))$ is made dimensionless by using a reference azimuthal velocity, W, which makes the dimensionless flowrate

upon the system cross section equal to 1. The Reynolds and Dean numbers are defined as $Re = W\ D_h/v$ and $Re\sqrt{D_h/R}$, respectively, where v is the kinematic viscosity of the carrier fluid and $D_h = 2H(1 - \kappa)/(\alpha(1 - \kappa) + 1)$ is the hydraulic diameter of the channel cross section, which for the chosen values of α and κ is equal to H.

Flow structure

The flow structure in curved ducts with squared cross section has been object of intense investigation (see, e.g., Mondal et al.,[20] and therein cited references). As regards the use of curved microchannels as passive mixing devices, an important parameter controlling mixing efficiency is the ratio of cross sectional to axial average velocity intensity.

Figure 2 depicts the ratio of the average Root-Mean-Square cross sectional to azimuthal velocity intensities $\Gamma = (\int_S (v_\rho^2 + v_\zeta^2)\ dS/\int_S v_\theta^2\ dS)^{1/2}$ averaged along a single mixer unit. As can be observed, the intensity of cross sectional velocity increases monotonically up to $De = 50$ and then oscillates about a value of order 10% of the azimuthal velocity intensity.

Given that at increasing De, the overall pressure drop through the mixer unit also increases and that at high Pe values, several mixing units are necessary for achieving efficient mixing, a low-to-moderate range of De, say $De \leq 100$, is a sensible starting point for investigating the performance of the S-shaped micromixer.

The numerical computation of the flow field was obtained through the StarCCM+ software suite, which uses a finite volume discretization of the Navier Stokes boundary value problem. A mixing device is typically composed of several units (e.g., order 10–20 units) connected in series. After a short spatial transient, one expects the flow to be spatially periodic, the period being a single S-shaped unit. The periodic solution was obtained as follows. For the first device unit, a Poiseuille profile at the inlet section was imposed. The three-dimensional flow within the device unit was then computed by specifying "Danckwerts' boundary conditions" (i.e., zero normal derivative of the velocity) at the outlet of the unit. The flow profile at the outlet of the first unit was then fed as an inlet condition for the second unit and so on. We found that the flow is essentially periodic already for the second device unit and is strictly periodic (to within machine error) at the third device unit. Therefore, the three-dimensional solution of the third device unit was assumed to be the representative block of the spatially periodic flow. In all of the simulations, no-slip conditions at the solid walls were assumed, which, in the case of liquid mixtures, are expected to be verified† whenever the characteristic dimension of the channel cross section is above 10 μm.[21] An overall pressure drop applied to the basic device unit is the driving force the creates the primary axial flow (i.e., along the azimuthal direction).

As base cases for the operating conditions, we henceforth consider the values $De = 10; 50; 100$. A detailed study of stability and bifurcations of Navier-Stokes flows in curved channels with square cross section has been recently discussed by Mondal et al.,[20] who showed that a steady solution continuously dependent on the De parameter characterizes the bifurcation diagram up to $De = 500$, which is well above the largest De number considered in this article. Specifically, up to $De = 100$, we find a steady solution characterized by a two-vortex structure with top-bottom cross sectional symmetry.

†The occurrence of slip velocity at static walls can be expected when the mean free path of the fluid molecules becomes comparable with the characteristic dimension of the cross section.

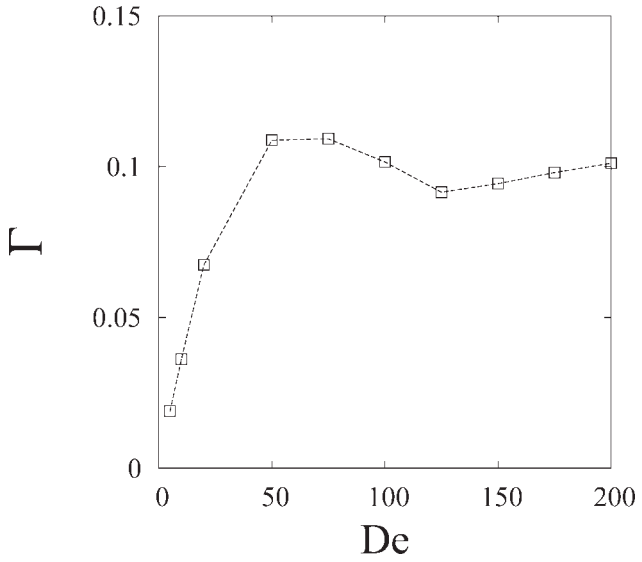

Figure 2. Average ratio of the cross sectional to azimuthal velocity intensity (see main text for details).

The convergence of the solution for different levels of discretization of the finite volume algorithm is depicted in Figure 3 where the velocity profiles at different values of the De number are represented along the horizontal and vertical axes of symmetry of the cross section at $\theta = \pi$ (denoted as S_1 in Figure 1) in the first mixer unit.

As can be observed, the velocity profiles are insensitive to increasing mesh resolution for the levels of discretization chosen. Henceforth, the mesh resolution for the CFD computation of the device unit is fixed at $N_{tot} = 32 \times 32 \times 768$.

A better visualization of the velocity field structure can be appreciated from the two-dimensional vector plots onto selected cross sections of the device. Figure 4 shows the cross sectional structure at the section S_1 of the fully developed spatially periodic flow, together with the contour plot of the axial velocity v_θ at $De = 10$ and 100. These results are in agreement with analogous computations reported in the Literature for the same system.[5] Note that at increasing De, the axial velocity magnitude (contour plot in the figure) looses symmetry with respect to vertical center-line of the cross section, as the point where maximum velocity is attained moves toward the boundary $\rho = 1$, physically representing the outer wall of the turn. As regards the cross sectional flow, which is normalized with respect to the axial reference velocity W and represented as vector plot, one notices the presence of a couple of weak counter-rotating vortexes at the lowest Dean number ($De = 10$), whose centers are nearly symmetric with respect to the vertical center-line of the cross section. At increasing De ($De = 100$), the vortex centers move toward the external wall and become more and more intense. The flow field in the second half unit is the symmetric reflection about the vertical center-line of that

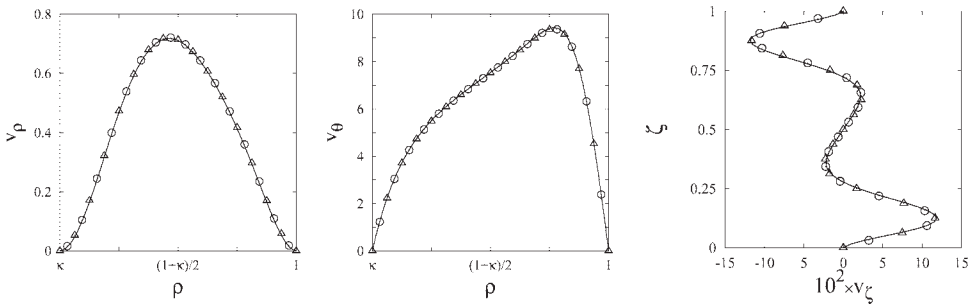

Figure 3. Velocity profiles at different mesh resolutions at *De* = 100.

The symbols and the continuous line are associated with different volume meshes, characterized by a total number of cells $N_{tot} = N_\rho \times N_\zeta \times N_\theta$; (Δ): $N_{tot} = 32 \times 32 \times 384$; (○): $N_{tot} = 32 \times 32 \times 768$; continuous lines: $N_{tot} = 64 \times 64 \times 384$. The profiles along the ρ coordinate are taken at $\zeta = 1/2$. The profiles along ζ are taken at $\rho = (\kappa + 1)/2$.

associated with the first half unit (not showed for brevity). Thus, to an observer moving downstream, the device axis with the average axial velocity, the cross sectional flow appears as a time-periodic, smoothly varying flow. This suggests that the kinematic behavior of trajectories at sufficiently large values of the *De* number might be chaotic. In point of fact, numerical evidence of chaotic behavior in the S-shaped micromixer has been found starting from $De = 100$.[14] The structure of the cross sectional flow depicted in Figure 4 is in good qualitative agreement with Literature data focusing on the same geometry.[5]

To make a more quantitative validation of the flow field, the simulation of flow trajectories associated with fluid particles that are fed along the vertical line of symmetry of the inlet section of a single device unit has been performed and compared with results obtained by Jiang et al.[14] for the same device geometry. It should be observed that such a comparison constitutes a very severe test for the CFD-computed velocity field in that small differences in the Eulerian pointwise structure of flow are summed up along the streamline integration and can lead to significant deviations of particle position downstream the mixer unit. This is particularly true at large *De* values, where the chaotic nature of the flow field can amplify exponentially small perturbations of fluid particle position. Figure 5 shows the result of such comparison at $De = 10$ and $De = 100$. Point positions on the inlet section spanned continuously the vertical line of symmetry in the upper half of the section. The intersection of the streamline passing through each inlet position with the cross sections at $\Theta = 3\pi/2$ and $\Theta = 3\pi$ were computed and compared with the results reported in the literature.[14] Streamline tracking was accomplished by trilinear interpolation, the velocity field in the cylindrical representation of the domain, and by integrating the flow trajectories with a fourth-order Runge-Kutta scheme. The data at $De = 10$ show an almost perfect agreement. The data at $De = 100$ show a good agreement, with small discrepancies that are most probably due to differences in the integration method. The good agreement provides a robust validation of the CFD computation.

Scalar Mixing in the Serpentine Channel

Advection-diffusion in open flows

With reference to the cylindrical coordinate system depicted in Figure 1 valid for a generic system half unit, which we henceforth denote simply as ρ, θ, ζ (dropping the subscripts), the dimensionless form of the steady-state advection-diffusion equation for the concentration, $\phi(\rho, \theta, \zeta)$ of a diffusing species carried by the flow can be written as

$$\frac{v_\theta}{\rho}\frac{\partial \phi}{\partial \theta} = -v_\rho \frac{\partial \phi}{\partial \rho} - \alpha v_\zeta \frac{\partial \phi}{\partial \zeta} + \frac{\alpha}{Pe}\left(\frac{1}{\alpha^2}\frac{\partial}{\rho \partial \rho}\left(\rho \frac{\partial \phi}{\partial \rho}\right) + \frac{1}{\alpha^2}\frac{1}{\rho^2}\frac{\partial^2 \phi}{\partial \theta^2} + \frac{\partial^2 \phi}{\partial \zeta^2}\right), \quad (3)$$

where $\rho \in [\kappa, 1]$, $\theta \in [0, 3\pi/2]$, and $\zeta \in [0, 1]$, and where the Peclet number is defined as $Pe = WH/\mathcal{D}$, $\mathcal{D}$ being the

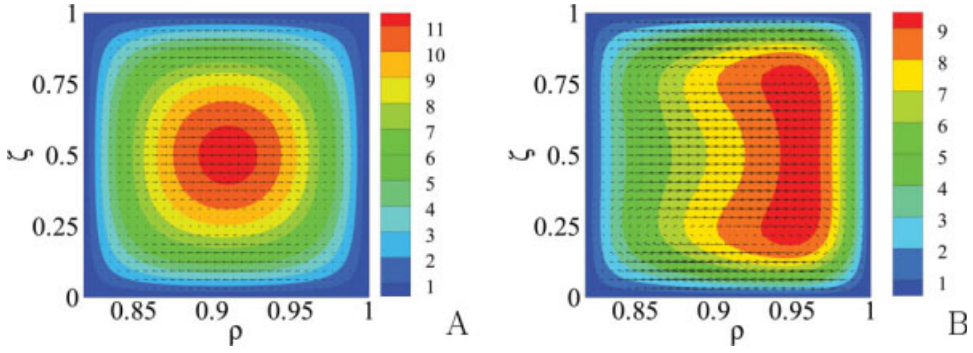

Figure 4. Structure of the cross sectional flow (vectors) and intensity of axial velocity (color contour) at the section S_1 (see Figure 1) for the fully developed spatially periodic flow.

Panel A, $De = 10$; Panel B, $De = 100$. [Color figure can be viewed in the online issue, which is available at www.interscience.wiley.com.]

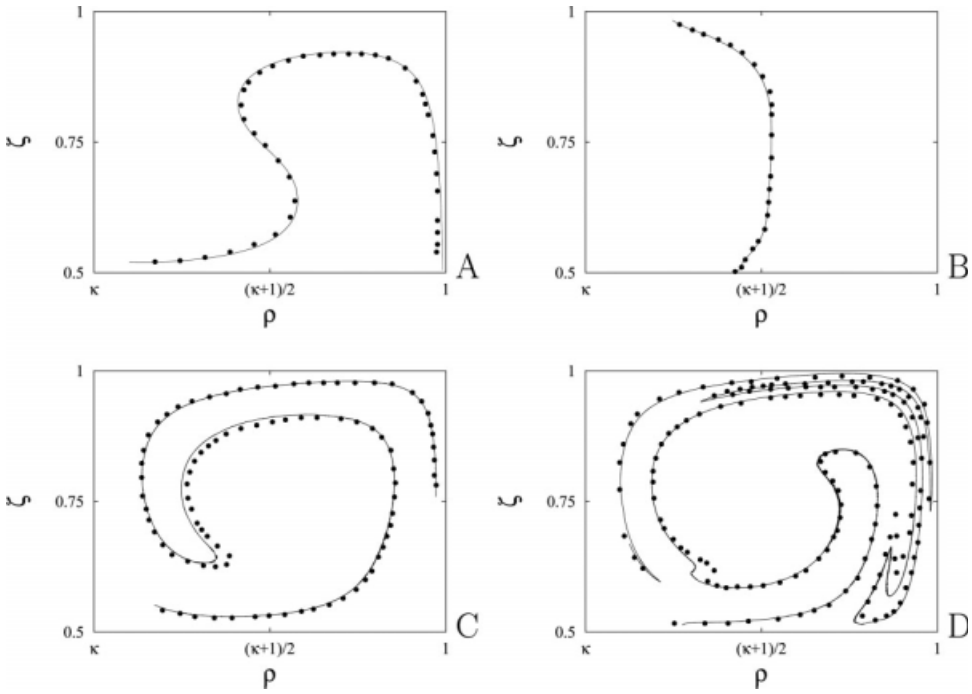

Figure 5. Comparison of kinematic structures with previously published data[14] at the end of the first and second half unit.

The continuous line represents the results of our simulation. Symbols (●) depict the data reported by Jiang et. al .[14] Panel A, $De = 10$, $\Theta = 3\pi/2$; Panel B, $De = 10$, $\Theta = 3\pi$; Panel C, $De = 100$, $\Theta = 3\pi/2$; Panel D, $De = 100$, $\Theta = 3\pi$. See main text for details.

diffusivity of the advected scalar. Since, by the choice of the geometric parameters α and κ discussed earlier, the hydraulic diameter of the channel is equal the channel height H, it results that $Pe = Re\ Sc$, where the Schmidt number Sc, denotes the ratio between the kinematic viscosity of the carrier flow to the molecular diffusivity of the species that is being mixed.

The velocity field appearing in Eq. (3) is assumed to be the fully developed spatially periodic flow discussed in the previous Section. Thus, here, we are neglecting the developing flow at the entrance of the first system unit, which depends on the specific entrance profile of the velocity field. However, theoretical estimates‡ and numerical results suggest that in laminar flows within curved channels, the entrance length, l_e, verifies the relationship $l_e = 0.1\ Re\ D_h$, where D_h is the hydraulic diameter of the cross section.[17] Thus, at the largest De value considered in this article, the flow can be considered fully developed already at $\theta_1 = \pi/2$.

Let us first analyze what is the relative importance of the three terms of the Laplacian between brackets at the r.h.s. of Eq. (3), by comparing the characteristic time for diffusion along each of the coordinate directions in the domain of interest. From Eq. (3), one observes that the dimensionless diffusion coefficients along the three-spatial coordinate directions ρ, θ, and ζ are equal to $D_\rho = (Pe\ \alpha)^{-1}$, $D_\theta = (Pe\ \alpha)^{-1}$, and $D_\zeta = (\alpha/Pe)$, respectively. The characteristic dimensionless lengths along the three spatial directions are given by $L_\rho = 1 - \kappa$, $L_\theta = 3\pi/2$, and $L_\zeta = 1$. Thus, the dimensionless times for diffusion in the first system half unit can be computed as $\tau_\rho^d = (1-\kappa)^2/D_\rho$ $\tau_\theta^d = (3\pi/2)^2/D_\theta$, and $\tau_\zeta^d = 1/D_\zeta$. Therefore, for the chosen values of α and κ, one obtains that $\tau_\rho^d/\tau_\zeta^d = 1$, and $\tau_\theta^d/\tau_\zeta^d = (3\pi/2)^2\alpha^2 \simeq 671$, which implies that there are almost three orders of magnitude of difference between the characteristic time for diffusion along θ and those associated with the system cross section. This observation suggests that axial diffusion can be neglected compared with cross sectional diffusion. With this approximation, Eq. (3) becomes

$$\frac{v_\theta}{\rho}\frac{\partial\phi}{\partial\theta} = -v_\rho\frac{\partial\phi}{\partial\rho} - \alpha v_\zeta\frac{\partial\phi}{\partial\zeta} + \frac{\alpha}{Pe}\left[\frac{1}{\alpha^2}\frac{\partial}{\rho\partial\rho}\left(\rho\frac{\partial\phi}{\partial\rho}\right) + \frac{\partial^2\phi}{\partial\zeta^2}\right], \tag{4}$$

Therefore, the process expressed by Eq. (4) is first order along the θ coordinate. The boundary value problem can then be posed by specifying the feeding condition $\phi_{in}(\rho, \zeta)$ at the inlet section, $\theta = 0$,

$$\phi_{in}(\rho,\zeta) = \phi(\rho,0,\zeta) = \begin{cases} \beta & \text{for} \quad \kappa \le \rho \le (\kappa+1)/2, \quad 0 \le \zeta \le 1 \\ -1 & \text{for} \quad (\kappa+1)/2 < \rho \le 1, \quad 0 \le \zeta \le 1, \end{cases} \tag{5}$$

and the usual impermeability conditions at the solid walls of the mixer, which impose zero diffusive flux of the scalar at these boundaries,

$$\nabla\phi \cdot \mathbf{n} = 0 \tag{6}$$

where $\mathbf{n}$ is a unit vector normal to the device wall at each point of the solid boundary.

‡The entrance length can be defined as the length downstream the channel such that the flow becomes independent of the structure of the inlet profile.

The parameter $\beta > 0$ appearing in Eq. (5) is such as to make the overall flow of the scalar equal to zero, so that the perfectly mixed condition achieved in an ideally infinitely long mixer is represented by a vanishing cross sectional scalar field. The departure of β from the value 1 compensates the fact that the periodicized velocity field is not strictly symmetric with respect to the vertical line of symmetry of the inlet cross section, especially when large *De* values are considered.

As azimuthal diffusion is assumed negligible, the matching condition for passing from the coordinate system ρ_n, θ_n, ζ_n, corresponding to a generic half unit to those associated with the the next half unit, ρ_{n+1}, θ_{n+1}, ζ_{n+1} is simply obtained by imposing continuity of the scalar field at the boundary cross section.

Mixing efficiency

Mixing in closed systems (i.e., bounded systems with impermeable boundaries) in the presence of a nonvanishing diffusivity — however small — is typically measured by the decay of the scalar field variance, which provides a global measure of the departure of the current state of the system from the uniformly mixed state. Because of the nature of the mixing space and to the presence of the Laplacian operator, it is straightforward to derive that the variance associated with any initial condition is always nonincreasing in time and is strictly decreasing whenever the initial scalar profile is not constant throughout space.

When open advecting-diffusing flows at steady state are to be dealt with, a common approach is to single out cross sectional mixing and analyze how the scalar variance decays when moving downstream the device axis. However, to keep a strict analogy with the case of closed system, both the cross sectional average of the scalar Φ and the scalar variance σ must be weighted by the azimuthal velocity v_θ, i.e.,

$$\Phi = \frac{\int_0^1 \int_\kappa^1 v_\theta \, \phi \, d\rho \, d\zeta}{\int_0^1 \int_\kappa^1 v_\theta \, d\rho \, d\zeta} \quad \sigma = \left[\frac{\int_0^1 \int_\kappa^1 v_\theta (\phi - \Phi)^2 d\rho \, d\zeta}{\int_0^1 \int_\kappa^1 v_\theta \, d\rho \, d\zeta} \right]^{1/2}, \tag{7}$$

where all the integral are evaluated at the constant θ value that identifies the cross section. Specifically, one can show that if azimuthal diffusion is neglected, Φ is conserved downstream the device (i.e., $\Phi = \text{const.}$), and if $v_\theta \geq 0$ for any θ, then the variance σ is a nonincreasing function of θ. Note that for the inlet condition expressed by Eq. (5), $\Phi = 0$, and therefore, the variance is just proportional to the velocity-weighted average of ϕ^2 onto the given section.

In this context, the mixing efficiency, $\eta(\Theta)$, along the device axis can be defined as

$$\eta(\Theta) = 1 - \frac{\sigma(\Theta)}{\sigma(0)}. \tag{8}$$

Spectral approach

The properties of Eq. (4) can be conveniently approached by means of the spectral characterization.[22,23] Let us first recall that for nonvanishing values of *De* (e.g., $De > 1$) all of the velocity components v_ρ, v_θ, v_ζ appearing in Eq. (4) depend strongly not only on the cross sectional coordinates ρ and ζ, but also on the streamwise coordinate θ. In brief, this equation could be regarded as describing transient mixing in a two-dimensional system by the action of a time-periodic velocity field. In this respect, the azimuthal variable θ is the analogous of a time variable, the two-dimensional mixing domain is the system cross section at constant θ, and the velocity field is given by the cross sectional velocity $\mathbf{v}_\perp = (v_\rho, v_\zeta)$. Besides, two specific features of Eq. (4) make it impossible to establish a strict correspondence between the two problems. The first is associated with the presence of a nonconstant function, namely the factor v_θ/ρ, multiplying the θ-derivative at the l.h.s. of Eq. (4). The second is that, unlike the case of transient mixing in a two-dimensional system, the cross sectional flow $\mathbf{v}_\perp$ need not be incompressible with respect to the cross sectional coordinates. Therefore, however qualitatively useful for guiding the design criteria of micromixers, the analogy should not be pushed too far, as differences might be expected between the two cases for the reasons discussed above.

Equation (4) can be expressed as

$$\frac{v_\theta}{\rho}\frac{\partial \phi}{\partial \theta} = -v_\rho \frac{\partial \phi}{\partial \rho} - \alpha v_\zeta \frac{\partial \phi}{\partial \zeta} + \frac{1}{Pe}\nabla_\perp^2 \phi = \mathcal{L}_\Theta^\perp[\phi], \tag{9}$$

where $\mathcal{L}_\Theta^\perp$ denotes a one-parameter family of operators-depending on the azimuthal coordinate Θ - henceforth denoted as cross sectional advection-diffusion operator, and

$$\nabla_\perp^2 = \alpha \left[\frac{1}{\alpha^2} \frac{\partial}{\rho \partial \rho} \left(\rho \frac{\partial}{\partial \rho} \right) + \frac{\partial^2}{\partial \zeta^2} \right] \tag{10}$$

is the cross sectional Laplacian. Stemming from the periodicity of the velocity field, it results that $\mathcal{L}_\Theta^\perp[\phi] = \mathcal{L}_{\Theta+3\pi}^\perp[\phi]$,, i.e., the family $\mathcal{L}_\perp^\Theta[\phi]$ is periodic modulo a single mixer unit. By the definition in Eq. (9), the family is uniquely identified whenever the three-dimensional flow within the mixer unit, and the *Pe* number have been specified. The explicit dependence of $\mathcal{L}_\Theta^\perp$ on the streamwise variable Θ makes the investigation of its properties different from previous studies of advection-diffusion in open systems at steady state,[23] simply because $\mathcal{L}_{\Theta_1}^\perp$ and $\mathcal{L}_{\Theta_2}^\perp$ do not commute for $\Theta_1 \neq \Theta_2$ modulo 3π.

In analogy with the case of closed time-periodic flows,[22], one can formally introduce a Poincaré or Floquet operator, say $\mathcal{F}[\phi]$. Consider the space of square summable functions $L^2(\Sigma)$ within the cross section of the device $\Sigma = \{(\rho, \zeta) | \kappa \leq \rho \leq 1, 0 \leq \zeta \leq 1\}$, and let $\mathcal{F} : L^2(\Sigma) \to L^2(\Sigma)$ the operator mapping $\phi^{(n-1)}(\rho, \zeta) = \phi(\rho, 3(n-1)\pi, \zeta)$ into $\phi^{(n)}(\rho, \zeta) = \phi(\rho, 3n\pi, \zeta)$, $n = 1, 2 \ldots$,

$$\phi^{(n)}(\rho, \zeta) = \mathcal{F}[\phi^{(n-1)}(\rho, \zeta)]. \tag{11}$$

The Floquet operator $\mathcal{F}$ so defined maps a cross sectional profile $\phi^{(n-1)}(\rho, \zeta)$ at the entrance of generic mixer unit, say $n = 1, 2, \ldots$ into the corresponding profile $\phi^{(n)}(\rho, \zeta)$ at the exit of that unit. For a mathematically sound definition, the class of functions acted upon by $\mathcal{F}$ should be made precise. Here we assume that the generic cross sectional profile is a square summable function defined on the cross section $\kappa \leq \rho \leq 1$, $0 \leq \zeta \leq 1$, i.e., that $\phi \in L^2(\Sigma)$, with vanishing normal

derivative at the cross section boundaries. The last condition stems from the boundary condition expressed by Eq. (6). As a consequence of the periodicity of v_θ and $\mathcal{L}^{\perp}_{\Theta}$ entering Eq. (9), $\phi^{(n)} = \mathcal{F}[\phi^{(0)}]$, where $F^{\mathrm{n}} = \underbrace{\mathcal{F}\mathrm{o}\cdots\mathrm{o}\mathcal{F}}_{n\ \text{times}}$ is the n-th power of $\mathcal{F}$, and "o" indicates operator composition.

Before describing how a finite-dimensional approximation of $\mathcal{F}$ can be obtained for an assigned velocity field and a specified value of Pe (see below), we next discuss how the spectral structure (eigenvalues-eigenfunctions) associated with the Floquet operator can be conveniently exploited for a quantitative assessment of mixing efficiency associated with a mixer device composed of several S-shaped units connected in a sequence. To this end, let λ and $X(\rho, \zeta)$ be an eigenvalue-eigenfunction of $\mathcal{F}$, thus satisfying the relationship

$$\mathcal{F}[X] = \lambda X. \tag{12}$$

It is commonly accepted that for a large class of flow fields, and any finite value of Pe, $\mathcal{F}$ admits a pure point countable spectrum of separated eigenvalues, $\{\lambda_h\}_{h\in\mathbb{N}}$, and that the corresponding eigenfunctions, say $\{X_h\}_{h\in\mathbb{N}}$, form a basis for the space of square summable functions (see, e.g., Ref. [22] and therein cited references). The eigenvalues-eigenfunctions are generally complex-valued, i.e., $\lambda_h = \mu_h\, \mathrm{e}^{(2\pi i q_h)}$ (μ_h is the modulus and $2\pi q_h$ the phase), and $X_h = X_h^{\mathrm{R}} + iX_h^I$, where i is the imaginary unit, $i = \sqrt{-1}$. In this framework, "pure point" means that there are no continuous portions of the spectrum (sometimes referred to as essential spectrum in the mathematical literature), whereas "separated" means that the set of eigenvalues admits no accumulation point different from the origin of the complex plane.[24] Furthermore, by the presence of the Laplacian term in the relationship that defines the family $\mathcal{L}^{\perp}_{\Theta}$, one derives that all of the eigenvalues are contained within the unit circle of the complex plane, $\mu_h = |\lambda_h| \leq 1$. Looking into the physical aspects, this property can be regarded as an ultimate consequence of the dissipative (irreversible) nature of molecular diffusion. Visual inspection of Eq. (12) shows that the (real) eigenvalue $\lambda_0 = 1$ with corresponding eigenfunction $X_0 = \text{Const.}$ belongs to the spectrum of $\mathcal{F}$. This eigenvalue-eigenfunction expresses the intuitive notion that a constant inlet profile is left unchanged by the cross sectional advection-diffusion process while it is being advected by the primary azimuthal flow downstream the mixer unit. Of course, this case is of no interest for mixing applications in that the inlet stream is already perfectly mixed. Henceforth, we assume that the eigenvalues spectrum is ordered such that $1 = \lambda_0 > \mu_1 \geq \ldots \geq \mu_h \geq \ldots$.

The physical significance of the spectrum can be readily appreciated as soon as one considers an expansion of a generic inlet profile in terms of eigenfunctions of $\mathcal{F}$,

$$\phi_{\mathrm{in}}(\rho, \zeta) = \phi^{(0)}(\rho, \zeta) = \sum_{h=0}^{\infty} C_h X_h(\rho, \zeta), \tag{13}$$

where the constants C_h ($h > 0$) are generally complex-valued and are uniquely specified by the function $\phi_{in}(\rho, \zeta)$. By the property that the convective scalar flux through any system cross section is conserved along the device axis, one derives that, by choosing $X_0 = 1$, the constant C_0 is given by

$$C_0 = \frac{\int_k^1 \int_0^1 v_\theta(\rho, 0, \zeta)\phi_{\mathrm{in}}(\rho, \zeta)d\rho d\theta}{\int_k^1 \int_0^1 v_\theta(\rho, 0, \zeta)d\rho d\theta} = \Psi \tag{14}$$

Thus, by defining a new variable $\overline{\phi} = \phi - \Phi$, one can always reduce to study the case where $C_0 = 0$. This physically corresponds to analyzing the approach to the constant homogeneous profile that would be obtained in an infinitely long mixer, where the value of the constant is given by the ratio of the average scalar flowrate to the overall volumetric flowrate. Henceforth, we assume that the inlet condition possesses vanishing C_0.

The inlet profile in Eq. (13) will be mapped at the exit of the n-th mixer unit into the profile $\phi^{(n)}(\rho, \zeta)$ given by

$$\phi^{(n)}(\rho, \zeta) = \sum_{h=1}^{\infty} C_h \lambda_h^n X_h(\rho, \zeta). \tag{15}$$

Note that the result of the mapping in Eq. (15) must be a real-valued function for any real function ϕ_{in}. This implies that all of the complex eigenvalues-eigenfunctions of the spectrum must always appear in complex-conjugate pairs.

Given that $\mu_h = |\lambda_h| < 1$ for $h \geq 1$, from Eq. (15) one gathers that for n large enough, the approach to the homogeneous profile $\phi^{(n)}(\rho, \zeta) = 0$ is controlled by the dominant eigenvalue λ_d, where d is the smallest integer such that $C_d \neq 0$. Two cases may arise, depending on whether the dominant eigenvalue-eigenfunction is real or complex. In the first case, the scalar profile at large values of n (i.e., at the exit of the n-th unit) decays as

$$\phi^{(n)}(\rho, \zeta) \sim C_d \mu_d^n X_d(\rho, \zeta), \tag{16}$$

and therefore the normalized function $\phi^{(n)}/\mu_d^n$ converges toward an n-invariant function. Besides, if the dominant eigenvalue-eigenfunction is complex, $\lambda_d = \mu_d\, e^{2\pi i q_d}$, $X_d = X_d^R + iX_d^I$, then the n-asymptotic behavior of the scalar profile, $\phi^{(n)}$ is given by

$$\phi^{(n)} = 2\mu_d^n\left[(A\psi_d^R - B\psi_d^I)\cos(2\pi q_d n) - (A\psi_d^I + B\psi_d^R)\sin(2\pi q_d n)\right], \tag{17}$$

where A and B are real constants, and therefore the spatial patterns of the normalized scalar field are periodic or quasiperiodic depending on whether q_d is rational or irrational.

From the above discussion, one gathers that the scalar variance, $\sigma(3\pi n)$, at the outlet section of the n-th mixer unit decays exponentially as

$$\sigma(3\pi n) = \text{Const.}\mu_d^n \tag{18}$$

Therefore, in a Θ-continuous framework, the scalar variance is expected to decay (with possible oscillations) about the exponential backbone

$$\sigma(\Theta) \sim \exp(-\Lambda_d \Theta), \quad \Lambda_d = -\log(\mu_d)/3\pi \tag{19}$$

As we are interested in connecting the spectral properties of $\mathcal{F}$ with the homogenization process downstream the

mixing device, for each eigenvalues $\mu_h e^{2\pi i q_h}$, we henceforth consider its rescaled value associated with the Θ-continuous frame, i.e.,

$$\Lambda_h = -\frac{\log(\mu_h)}{3\pi}, \quad h = 0, 1, \ldots \tag{20}$$

Numerical issues

To obtain a finite-dimensional approximation of the Floquet operator, a suitable basis for representing the functional space $L^2(\Sigma)$ must be chosen, say $\{Y_h(\rho, \theta)\}_{h\in\mathbb{N}}$, where $Y_h(\rho, \theta)$ is a generic basis function satisfying Neumann conditions on the boundary of the cross section. In the chosen basis, the Floquet operator is represented by an infinite-dimensional square matrix. Amongst the possible choices of $\{Y_h(\rho, \theta)\}$, two broad categories can be identified, namely, localized§ basis functions such as those exploited in finite-volume and finite-elements methods, or global basis functions, such as the eigenfunctions of the Laplacian operator. Localized approaches present the advantage of simple implementation even in complex geometries, especially when used in combination with automatic mesh-generating algorithms. Besides, their main shortcoming is that they are subject to numerical diffusion at large values of the *Pe* number, which forces to consider a very large number of basis functions (i.e., a fine discretization of the domain), especially when three-dimensional flows are to be dealt with. On the other hand, approaches based on global basis functions are known to be less prone to numerical diffusion issues; howerer, their practical implementation is limited to the cases of domains with simple geometries. By exploiting the simple structure of the system cross section, we choose the Fourier cosine representation as a basis, i.e.,

$$Y_{m,n}(\rho, \zeta) = \cos\left(m\pi\frac{\rho - \kappa}{1 - \kappa}\right)\cos(n\pi\zeta), \tag{21}$$

where the maximum number number of modes $M = M_\rho \times M_\zeta$ varied from a mininum of $M = 20 \times 20$ to a maximum of $M = 50 \times 50$ for the lowest and largest value of *Pe* considered, respectively. To obtain a representation of the field in this basis, the nodal values of the velocity components must be interpolated to define a pointwise velocity field.We used bilinear interpolation on the two dimensional cross sectional grid for all of the velocity components, whereas a piecewise constant structure within each cell along the azimuthal direction Θ was assumed. With this assumption, the evolution of the scalar field along Θ is approximated through a sequence of piecewise Θ-independent flows. Therefore, in the region comprised between the cross section Θ_k and $\Theta_k + \Delta\Theta$ (where $\Delta\Theta = 3\pi/N_\Theta$, $N_\Theta = 768$), the variation of the scalar field along θ is given by the linear system of ODE

$$\frac{d\mathbf{f}}{d\theta} = \mathbf{B}_k^{-1}\mathbf{C}_k\mathbf{f} = \mathbf{A}_k\mathbf{f}, \quad \Theta_k \le \Theta < \Theta_{k+1}, \tag{22}$$

where $\mathbf{f} = (f_1, f_2, \ldots, f_M)^t$ (the superscript t denotes the transpose operation, i.e., $\mathbf{f}$ is a column vector) represents the coefficients of expansion of the cross sectional scalar profile, and where the entries of the $M \times M$ matrices $\mathbf{B}_k = (B^k_{(p,q),(m,n)})$ and $\mathbf{C}_k = (C^k_{(p,q),(m,n)})$ can be computed by quadratures and depend on the cross sectional flow and on the assigned value of *Pe* considered:

$$B^k_{(p,q),(m,n)} = \int_\Sigma v_\theta Y_{p,q} Y_{m,n} d\rho d\zeta|_{\Theta=\Theta_k} \tag{23}$$

$$C^k_{(p,q),(m,n)} = \int_\Sigma Y_{p,q}\left[-v_\rho\frac{\partial Y_{m,n}}{\partial\rho} - \alpha v_\zeta\frac{\partial Y_{m,n}}{\partial\zeta} + \frac{1}{Pe}\nabla_\perp^2 Y_{m,n}\right]\rho d\rho\, d\zeta\Big|_{\Theta=\Theta_k} \tag{24}$$

Equation (22) is complemented with the initial condition $\mathbf{f}(\theta = 0) = \mathbf{f}_0$, where the components of $\mathbf{f}_0$ are the coefficients of expansion of the cross sectional profile at $\Theta = \Theta_k$. Therefore, the iteration of the systems Eq. (22) allows to determine the scalar profile at a generic cross section starting from the expansion of the inlet condition at the entrance of the first mixer element.

Given the family of matrices $\mathbf{A}_1,\ldots,\mathbf{A}_{N_\Theta}$, the Floquet operator can be computed analytically as the product of matrix exponentials

$$\mathcal{F} = \exp(\mathbf{A}_{N_\Theta}\Delta\Theta)\cdot\exp(\mathbf{A}_{N_\Theta-1}\Delta\Theta)\cdots\exp(\mathbf{A}_1\Delta\Theta) = \sum_{k=0}^{N_\Theta-1}\exp(\mathbf{A}_{N_\theta-k}\Delta\Theta).$$

Note that the (left) composition of exponentials in Eq. (25) is not equivalent to the exponential of the sum of the operators in that two generic operators $\mathbf{A}_k$ and $\mathbf{A}_{k'}$ at different values of the axial coordinate (i.e, $k \neq k'$) typically do not commute.

Results

Operating conditions and typical ranges of Sc and Pe

In the fluid dynamics Literature focusing on the fundamental properties of the advection-diffusion equation, the analysis of the interaction between convective mixing (be it regular or chaotic) and molecular transport is typically pursued by considering the behavior of mixing performance for fixed flow conditions and increasing values of the *Pe* number (see, e.g., Refs. 19,22,25,26). In S-shaped micromixer, this physically corresponds to investigate, at fixed *De* number, the capability of the device to mix species of decreasing molecular diffusivity. However, if the comparison between the mixing performance of a prescribed fluid stream (i.e., characterized by a given Schmidt number, *Sc*) at different *De* values is sought, then the Peclet number should be varied according to $Pe = Re\ Sc$. In principle, both type of experiments are worth being considered, and in the presentation of the results, we discuss separately the two cases. As a reference interval for the Schmidt number we consider $1 \le Sc \le 10^3$, which ranges from the typical values of a rarefied gas to those associated with simple molecules diffusing in a liquid mixture. Although higher values of *Sc*, e.g., $Sc \in (10^4, 10^6)$ are not uncommon in specific applications (especially

§Here localized means compactly supported functions, i.e., functions that are different from zero only on a compact subdomain of the cross section.

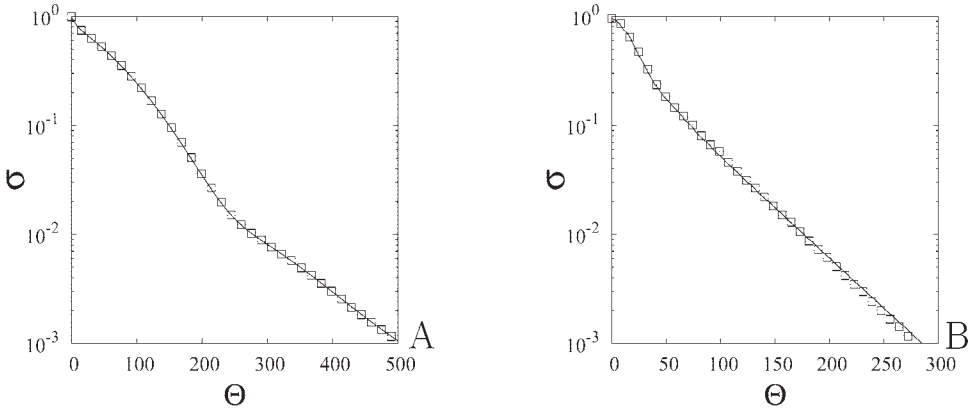

Figure 6. Validation of the numerical approach for solving the transport problem.

Behavior of the scalar variance $\sigma(\Theta)$ vs. Θ at different number of Fourier modes $M = M_\rho \times M_\zeta$. Panel A, $De = 10$, $Pe = 2.1 \times 10^4$; Panel *B*, $De = 100$, $Pe = 2.1 \times 10^5$. Symbols (□) and solid lines correspond to $M = 30 \times 30$ and $M = 50 \times 50$ Fourier modes, respectively.

those involving biomolecules and cell suspensions[3]), we refrain from exploring this *Sc* range in that the numerical solution of the transport problem at the corresponding *Pe* values becomes computationally prohibitive both in terms of memory capacity and CPU time.

We begin our discussion by considering the scalar variance downstream the mixing device, which characterizes the distance from the perfectly homogeneous condition.

Scalar variance decay and mixing efficiency

First, we seek for an estimate of the minimum number of Fourier modes, $M = M_\rho \times M_\zeta$ that is necessary to represent accurately the transport process. Figure 6 shows the behavior of scalar variance decay associated with the inlet condition expressed by Eq. (5) at $De = 10$, $Pe = 2.1 \times 10^4$ and $De = 100$, $Pe = 2.1 \times 10^5$ (which correspond to $Sc = 900$), for different values of the number of Fourier modes M. As can be observed, at both *De* values, increasing M from $M = 30 \times 30$ to $M = 50 \times 50$ does not cause any appreciable change in the azimuthal profile of $\sigma(\Theta)$.

On the basis of these results, we fixed the range of M from $M = 30 \times 30$ for the lowest *De* and lowest *Pe* considered, to $M = 50 \times 50$ for $De = 100$ and $Pe = 2.1 \times 10^5$.

Let us then analyze the behavior of scalar variance decay at fixed fluid dynamic conditions while varying the Peclet number. Panels A, B, and C of Figure 7 depict $\sigma(\Theta)$ vs Θ at different *Pe* values for $De = 10$, 50, 100, respectively. At the lowest *De* number (Figure 7A), the variance decays strictly exponentially at low *Pe* values (triangles (▽) and delta (Δ) symbols), whereas a rather long spatial transient (order of $\Theta = 250$, corresponding to more than 20 units) characterizes the intermediate *Pe* value — represented by circles (○) — before the exponential decay settles in. At the highest value of *Pe* (square symbols (□)), an oscillating behavior about a strictly exponential backbone can be observed. When the *De* number is increased, the approach to homogeneous conditions is faster and faster (compare the ranges of Θ of Figure 7B,C with those of Panel A). Also note that when the intensity of the cross sectional flow increases with respect to the axial flow (i.e., when *De* is increased, see Figure 2), the spatial transient to reach an overall exponential decay becomes shorter (e.g., the transient is order of $\Theta = 40$ at $De = 100$ and $Pe = 10^5$, which corresponds to about 4 mixer units). If we fix a variance of order $\sigma = 10^{-2}$ as a target mixing requirement (the so-called 99% mixing condition) and $Pe = 2.1 \times 10^4$, then the data of Figure 7 indicate that dimensionless lengths of order $\Theta = 400$, $\Theta = 200$, and $\Theta = 100$ are necessary to achieve the prescribed level of mixedness at $De = 10$, $De = 50$, $De = 100$, respectively. The increased mixing efficiency at increasing *De* values finds qualitative correspondence with the degree of chaos that characterizes the kinematic performance of the mixer, which passes from a substantially kinematically regular behavior at $De = 10$, to a condition where the chaotic region occupies a significant portion of the mixer cross section (and the kinematic interface is stretched exponentially fast in Θ, Ref. [14]) at $De = 100$. We stress out that such correspondence is qualitative in that, for the range of *Pe* values considered, mixing performance still appears to be very far from the ideal behavior where mixing efficiency becomes almost independent of the *Pe* number, which characterizes mixing performance of closed globally chaotic flows at vanishing values of the molecular diffusivity.[18,27] A partial if qualitative support to the idea that steady state mixing along an inflow–outflow device can be different from transient mixing in closed systems, especially as regards the connection with the kinematic performance of the flow, is suggested by the analysis of the partially mixed structures with and without molecular diffusion. Figure 8 shows this comparison at $De = 50$ and $Pe = 2.1 \times 10^4$. Panels A and B depict the kinematic structures in the upper half of the cross section associated with the initial condition expressed by Eq. (5) half way through, and at the exit of the first mixing unit, respectively. Panels C and D represent the mixing structures for the same inlet condition at $Pe = 2.1 \times 10^4$ (corresponding to $Sc = 500$). Half way through the first unit, the presence of diffusion does not alter substantially the structure of mixing patterns. However, already at the end of the first unit (Panels B and D), the mixing patterns bear very little relationship with each other. It is important to remark that the departure from the purely kinematic limit has here occurred

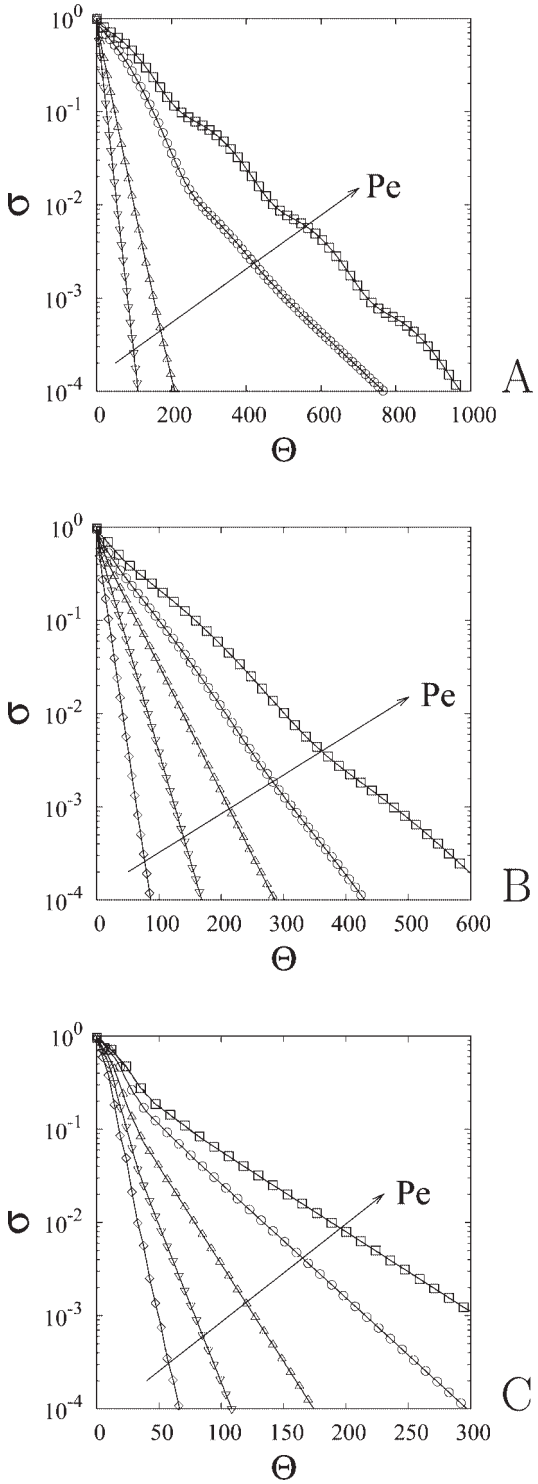

Figure 7. Scalar variance vs Θ at different *Pe* and fixed *De* number.

Panel A: $De = 10$. (□), (○), (Δ), and (△) correspond to $Pe = 4.2 \times 10^4$; 2.1×10^4; 4.2×10^3; 2.1×10^3, respectively. Panel B: $De = 50$. (□), (○), (Δ), and (◇) correspond to $Pe = 10^5$; 4.2×10^4; 2.1×10^4; 10^4; 4.2×10^3, respectively. Panel C: $De = 100$. (□), (□), (Δ), (▽) and (◇) correspond to $Pe = 2.1 \times 10^5$; 10^5; 4.2×10^4; 2.1×10^4; 10^4, respectively. Arrows indicate increasing *Pe* values.

at the early stages of the process, when very little mixing has taken place. The analysis of the mixing structures after three and five mixing units (Panels E and F, respectively) shows that, in the present case, the cross sectional field undergoes mixing while substantially maintaining the same geometric patterns.

Let us next analyze the dependence of mixing performance on the *De* number at fixed values of the Schmidt number. Figure 9 shows the dependence of the mixing efficiency $\eta(\Theta)$ vs Θ at $De = 10$, 50, and 100. The best performing flow condition is clearly $De = 100$, for which 99% mixing is achieved in less than 20 mixer unit. The cases $De = 50$ and $De = 10$ perform similarly, with and overall efficiency that is slightly above 90% mixing at the end of the 20th unit. The $De = 50$ protocol results slightly more efficient up to $\Theta \simeq 150$, where it intersect the curve associated with $De = 10$. At higher values of Θ, the $De = 10$ protocol mixes slightly better. This seemingly counter-intuitive result can be readily explained by considering that keeping the Schmidt number constant implies that *Pe* must increase proportionally to *De*, and therefore, the curves refer to different *Pe* values. In fact, a fair comparison of efficiency should also take into account that the volume flowrate at $De = 50$ is five times greater than that at $De = 10$, which means that five times more material is processed in the unit time within the same device at $De = 50$ with respect to the $De = 10$ case. This observation is made intuitively clear by analysis of the partially mixed structures in the two cases, which are depicted in Figure 10. As can be observed, the scalar fields associated with the higher value of *De* are characterized by a finer detail of structures with respect to the case of $De = 10$, where the patterns are essentially arranged in a two-lobe geometry. However, the higher *Pe* value associated with $De = 50$ flow makes the survival of small lamellae possible at the cross sections considered, with the result that the mixing process is far from ensuring a homogeneous condition, even in the presence of a more efficient cross sectional flow.

Spectral structure

Next, let us consider the spectral structure of the Floquet operator $\mathcal{F}$, which describes the mixing process at multiple integers, $\Theta_n = 3\pi n$, of the azimuthal length of the device unit. To compare the spectral properties of $\mathcal{F}$ with the decay of the scalar variance in a Θ-continuous framework, throughout the remainder of the article all of the eigenvalues are rescaled according to Eq. (20).

Let us first analyze the numerical issues regarding the computation of the spectrum associated with a truncated representation of the Floquet operator, as discussed at the end of the previous Section , where the discretization along the azimuthal coordinate Θ is fixed at $\Delta\Theta = 3\pi/768$. Figure 11 shows the behavior of the first and second eigenvalue, Λ_1 and Λ_2 at different resolutions of the number of modes, ranging from $M = 30 \times 30$ to $M = 50 \times 50$ at the highest Dean value considered, $De = 100$ as a function of *Pe*. In the low *Pe* range, results are unambiguously insensitive to increasing resolution for both Λ_1 and Λ_2, whereas at large *Pe* the dominant eigenvalue Λ_1 displays a nonmonotonic convergence (note that the data at $M = 30 \times 30$ and $M = 50 \times 50$ essentially coincide, whereas the data at $M = 40 \times$

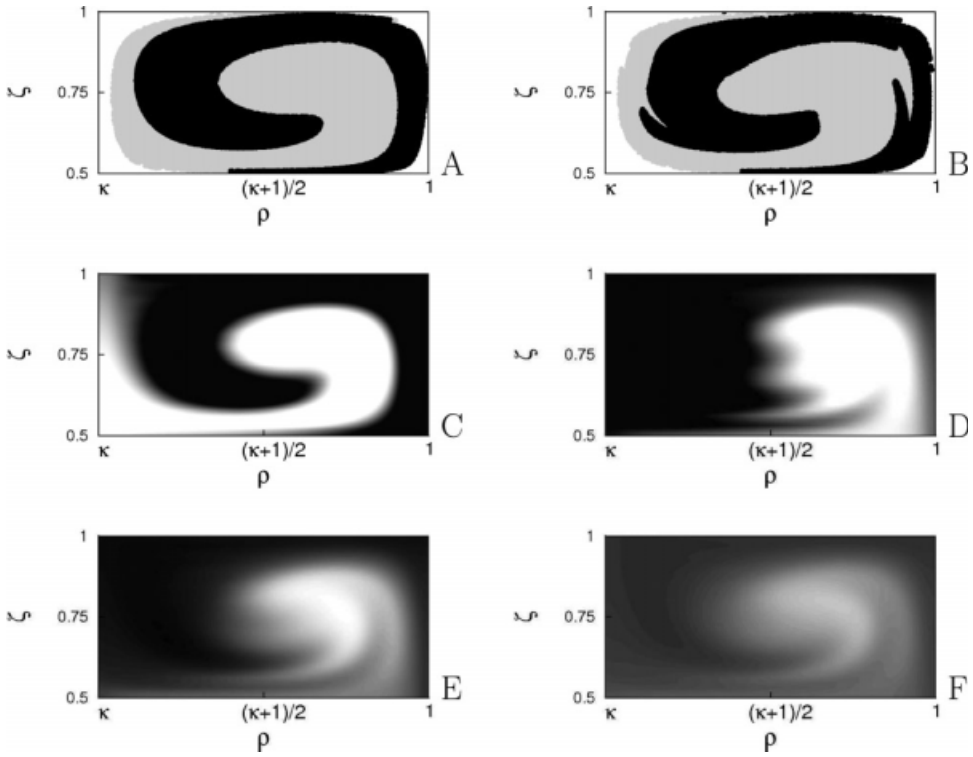

Figure 8. Comparison between partially mixed structures with and without molecular diffusion for an inlet condition expressed by Eq. (5), corresponding to the two segregated streams each occupying one of the vertical halves of the cross section.

Panels A and B represent the kinematic structures at $\Theta = 3\pi/2$ and $\Theta = 3\pi$, respectively. Panels C, D, E, and F represent the concentration field at $De = 50$, $Pe = 2.1 \times 10^4$ for $\Theta = 3\pi/2$, $\Theta = 3\pi$, $\Theta = 9\pi$, $\Theta = 15\pi$. The contour levels span the interval $(-0.5,0.5)$. Black and white correspond to positive and negative values, respectively. Note that the similarity of the scalar contour with the kinematic structure (Panels A and C) is lost already at the end of the first mixer unit (Panels B and D).

40 appear to overestimate Λ_1). As a result of the convergence tests, we fixed $Pe = 2.1 \times 10^5$, which at $De = 100$ corresponds to a Schmidt number of order 10^3, as the highest Pe value for which $M = 50 \times 50$ Fourier modes still provide accurate results. Figure 12 shows the behavior of the first eight eigenvalues as a function of Pe for the three values of De. In each panel of the figure, the dashed line represents the slope -1 associated with a purely diffusive scaling, $\Lambda \approx$ Const./Pe, i.e., to the scaling behavior of Λ vs Pe that would be observed in an inflow–outflow systems where no cross sectional flow is present. Therefore, any deviation from this scaling can be regarded as a convection enhancement to mixing, and in point of fact the wording convection-enhanced mixing regime has been generically used to refer to all the cases where the slope of the curve $\Lambda(Pe)$ deviates significantly from the value -1.[18,22,23]]. Several observations are worth being made when comparing the spectra at different flow conditions.

Let us begin with the case of $De = 10$ (Figure 12A). Here almost all of the eigenvalues scale essentially diffusively with Pe, with the exception of the first eigenvalue, Λ_1 which at large Pe values appears to approach a convection-enhanced scaling. At $De = 50$, the departure of Λ_1 from a diffusive scaling settles in at slightly lower Pe values, whereas the upper part of the spectrum scales nearly diffusively. Note, however, that at large Pe the second and third

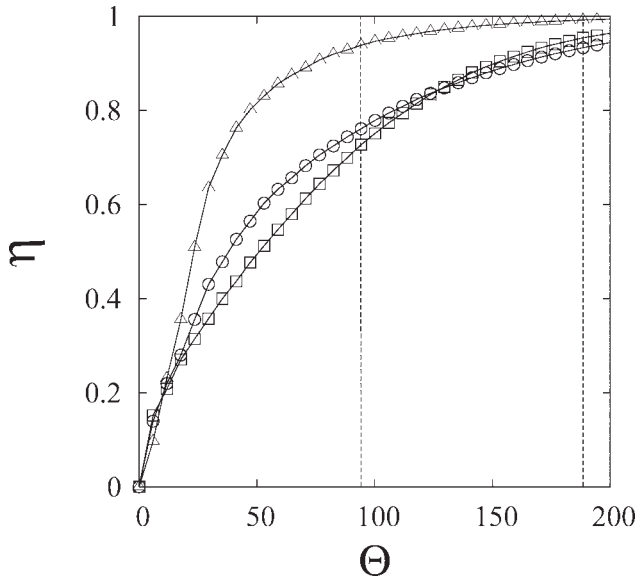

Figure 9. Mixing efficiency at different *De* values and fixed Schmidt number, *Sc* = 900.

The symbols (□), (○), and (Δ) correspond to $De = 10$; 50; 100, respectively. The vertical dashed lines indicate the Θ values corresponding to the end of the 10th and 20th mixer unit.

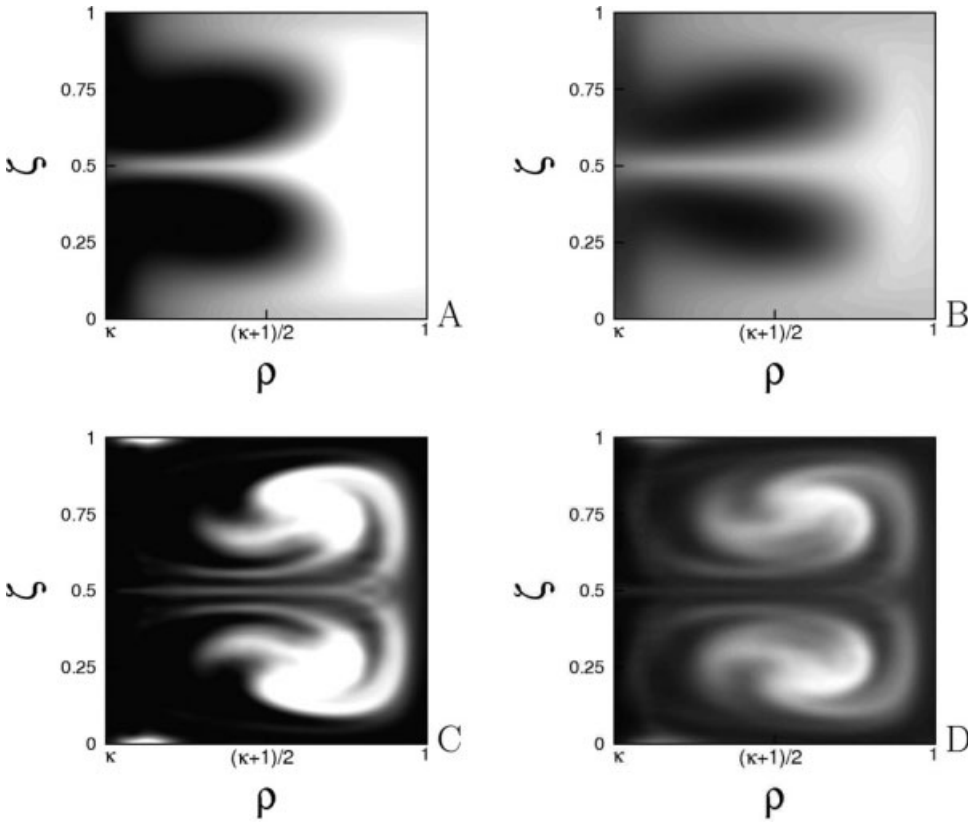

Figure 10. Cross sectional scalar profiles at *Sc* = 900 and different *De* values at Θ = 15π (left column - end of the fifth unit) and Θ = 30π (right column - end of the tenth unit).

Panels A and B, $De = 10$; Panels C and D, $De = 50$. Contour levels are the same as in Figure 8.

eigenvalues are significantly larger than those associated with the case $De = 10$. Thus, an inlet condition that possesses null component on the first eigenmode (i.e., such that $C_1 = 0$) is expected to mix more efficiently at $De = 50$ than at $De = 10$ at the same Pe value. At the largest Dean value ($De = 100$, Figure 12C), the scaling of the first eigenvalue appears substantially analogous to the other flow conditions, whereas a significant enhancement of mixing regimes is clearly appreciable in the upper part of the spectrum. For instance, at the largest Pe considered, there is almost an order of magnitude difference between the second eigenvalue at $De = 10$ and $De = 100$.

Let us finally analyze how the spectra associated with different De numbers compare with each other as a function of the Schmidt number. As discussed earlier, the mixing performance of different flows at the same Sc correspond to an experiment where the flowrate is increased while keeping the physical properties of the process stream constant. Panels A to C of Figure 13 show, such comparison for the first, second, and third eigenvalue, respectively. For the first eigenvalue, the best performing protocol at any Sc is always that associated with $De = 10$. As already observed, this is not surprising, the residence time decreases proportionally to De when maintaining a fixed Sc number. Besides, when attention is focused on the second and third eigenvalues (Figure 13B,C), the situation is rather different. At low Sc (e.g., at typical values associated with gaseous mixtures), the

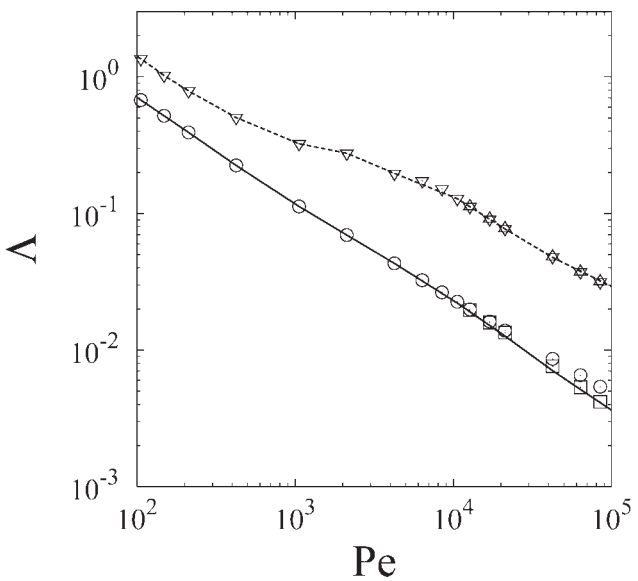

Figure 11. First and second eigenvalues, Λ_1 and Λ_2 at different resolutions of Fourier modes $M = M_\rho \times M_\zeta$ at $De = 100$.

Continuous line: Λ_1 at $M = 30 \times 30$. (○): Λ_1 at $M = 40 \times 40$ (□): Λ_1 at $M = 50 \times 50$; (○): Λ_1 at $M = 30 \times 30$. Dashed line: Λ_2 at $M = 30 \times 30$. (▽): Λ_2 at $M = 40 \times 40$; (◁): Λ_2 at $M = 50 \times 50$.

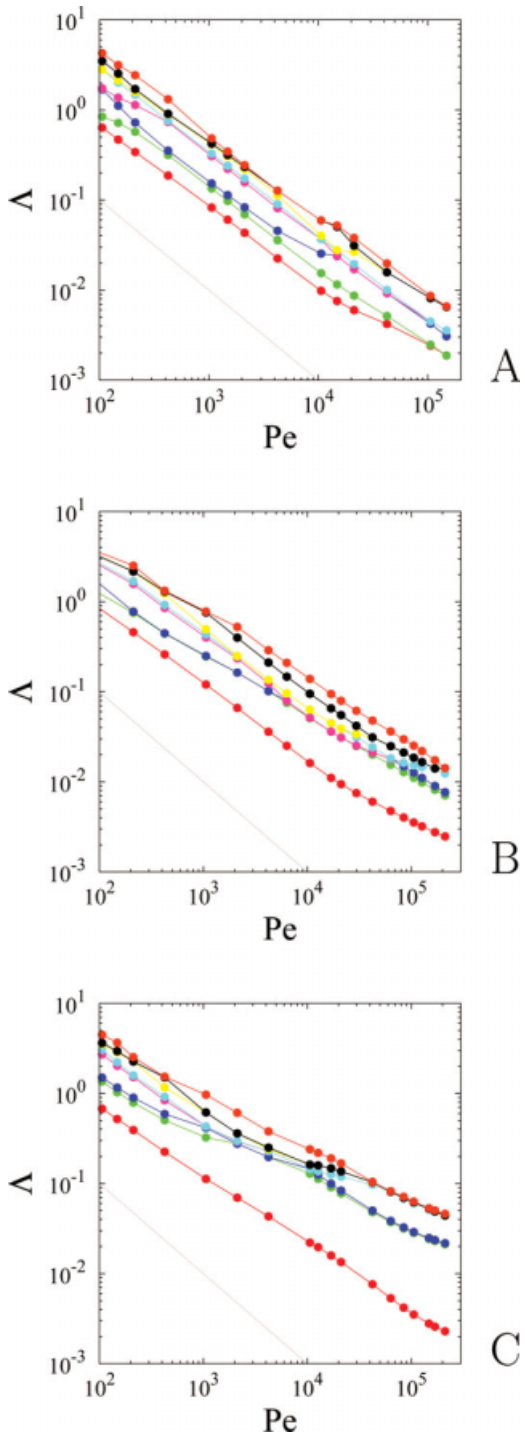

Figure 12. First eight eigenvalues, Λ_1 to Λ_8, at different values of the Dean number.

Panel A, B, and C, depict $De = 10$, 50, and 100, respectively. [Color figure can be viewed in the online issue, which is available at www.interscience.wiley.com.]

behavior is essentially analogous to that of the first eigenvalue. However, at values of the Schmidt number that are relevant for liquid mixing, the enhancement to the upper part of the spectrum due to cross sectional flow is so pronounced to overcome even the ten-fold decrease of residence time and yield a better mixing performance notwithstanding the higher flowrate.

Discussion. Connecting Spectral Properties to Mixing Efficiency

The discussion of the results developed above suggest that there is a qualitative correspondence between the spectral

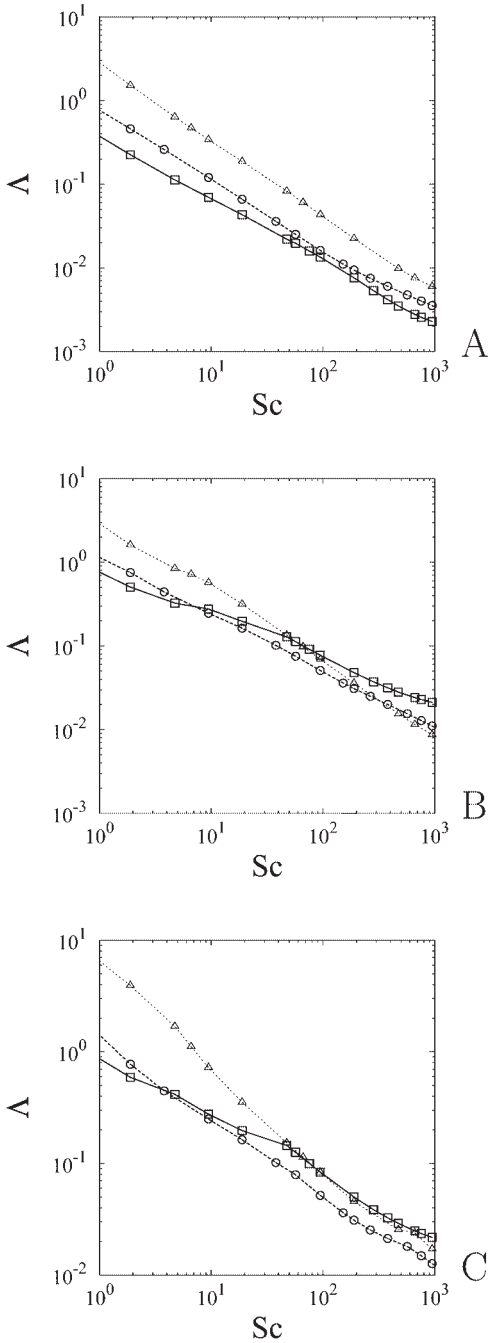

Figure 13. Comparison of the first three eigenvalues, Λ_1, Λ_2, and Λ_3 at different *De* values as a function of *Sc*.

Panels A, B, and C depict Λ_1, Λ_2, and Λ_3, respectively. (□), $De = 100$; (○), $De = 50$; (△), $De = 10$.

properties of the Floquet operator $\mathcal{F}$ and mixing efficiency associated with a typical experiment, such as that defined by the inlet conditions expressed by Eq. (5). Before trying to make this connection more explicit, which is the main scope of this Section, we want discuss what are the limits of a direct approach to the characterization of mixing and what are the advantages of pursuing a spectral analysis.

Beyond the classical Residence-Time-Distribution approach, there are to date two different ways for assessing mixing efficiency in inflow-outflow systems operating at steady state, namely, a kinematics-based characterization and the mixing-time analysis.

Kinematic approach

By the specific nature of the quantities that are used to define mixing efficiency (ultimately related to the infinitesimal deformation process of line and surface elements advected by the flow), the kinematic characterization relies almost esclusively upon numerical simulations. In the Introduction, we highlighted what are the limitations associated with this approach. Here, we can narrow the discussion and make it more precise within the framework of steady-state mixing in open devices. The main legacy from the investigation of closed flow systems in the presence of Lagrangian chaos is that the mixing ideal is constituted by a globally chaotic flow, which can stretch exponentially fast line and surface elements anywhere in the flow domain. From the spectral standpoint, this ensures that the dominant eigenvalue of the Floquet operator (which, for transient mixing in closed flows, is defined over a *time-period*) scales singularly with *Pe*, i.e., it saturates toward a constant value different from zero in the limit where *Pe* diverges to infinity.[22] Therefore, the ultimate interaction (i.e., at sufficiently large times) between advection and diffusion in closed globally chaotic flows is such as to yield a performance that is independent of the diffusivity value, however small. Based on this result, and assuming a qualitative equivalence between cross sectional mixing downstream an open device and transient mixing in closed domain, a number of strategies have been devised to promote globally chaotic conditions in laminar static mixers whose dimensions fall in the ordinary length-scale domain. In this case, the kinematics-based optimization of the device is supported by the observation that at values of the Reynolds numbers that fall in the range considered in this article, the *Pe* number associated with a static mixer of ordinary lengthscale is several orders of magnitude higher with respect to that associated with a microflow.¶ At these values of *Pe* numbers, one may assume that the asymptotic singular scaling has already settled in.

Besides, the data presented in the previous Section suggest that in the *Pe* interval associated with typical *Sc* values of liquid mixtures in a prototypical micromixer, the scaling behavior of the spectrum may be still far away from the singular scaling associated with globally chaotic conditions, even provided that such scaling does occur in an open flow.

¶Typical laminar flows in static mixers are associated with highly viscous flows (e.g. glycerol), whose kinematic viscosity is three orders of magnitude higher w.r.t. aqueous solutions.

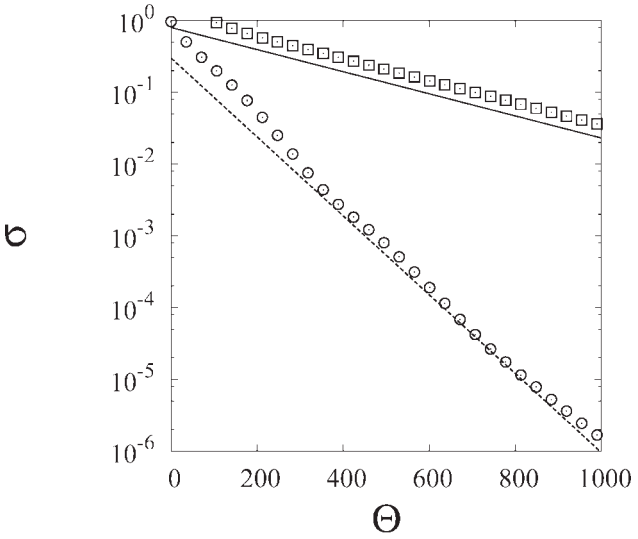

Figure 14. Variance decay for different inlet conditions and its relationship with the first two eigenvalues of the spectrum.

(□), continuous injection feeding (Dirac's delta distribution) at $\rho = 2(\kappa + 1)/3$, $\zeta = 0.3$, (○), segregated feeding condition [Eq. (5)]. The continuous and dashed lines depict the exponential decay associated with the first and third eigenvalue, $\Lambda_1 = 0.00355$ and $\Lambda_3 = 0.01265$, respectively.

Mixing time

The mixing time is the most straightforward and physically sound approach to the quantification of mixing efficiency. In steady-state inflow–outflow devices, the concept of mixing time really corresponds to a device length to obtain a prescribed level of mixedness (quantified by the scalar variance); however, it is customary to represent the data in terms of a scaled time obtained by dividing the mixing length by the average flow velocity. Despite its wide use, also because of a direct experimental feasibility of the measure, the major shortcoming associated with the mixing time is its strong dependence on the specific realization of the mixing process, i.e., in the present case, on the choice of feeding condition. As an illustrative example, Figure 14 shows the variance decay for two different feeding conditions at $De = 50$ and $Pe = 10^5$. The fast-decaying curve, depicted by (○) symbols, represents the segregated feeding condition of Eq. (5), whereas the slow decaying case is associated with a continuous injection of tracer at a point of the inlet section. Note that in the latter case, the mathematical representation of the feeding condition is given by a Dirac's delta distribution, which is not square summable at $\Theta = 0$, because of to the presence of the Laplacian term in the advection-diffusion process, the cross sectional profile at any positive Θ value possesses finite variance. The data make it evident that the estimate of mixing time can be strongly dependent on the feeding condition. For instance, the Θ value necessary to reach 99% mixing is of order 300 for the fast decaying condition, whereas is well above $\Theta = 10^3$ for the continuous injection. The lines next to the (□) and (○) symbols represent the prediction based on the first and third eigenvalue, respectively, i.e., $\sigma(\Theta) = e^{-\Lambda_1\Theta}$ and $\sigma(\Theta) = e^{-\Lambda_3\Theta}$.

As can be noted, the different initial conditions select different eigenfunction-eigenvalues from the spectrum, meaning that while the dominant eigenvalue is Λ_1 for the continuous injection which does not possess any specific symmetry, the symmetric structure of the segregated feeding condition projects onto the third eigenspace of the Floquet operator. This can be readily explained by the symmetry properties of the eigenfunctions. Consider, for instance, the first eigenfunction, $X_1(\rho, \zeta)$ of the Floquet operator (Figure 15), which, for the chosen values of *De* and *Pe*, is real-valued together with the corresponding eigenvalue Λ_1. As can be observed, the first eigenfunction possesses the symmetry $X(\rho, \zeta) = -X(\rho, 1 - \zeta)$, which implies that the projection coefficient C_1 is equal to zero when the segregated inlet condition Eq. (5) is considered. Note that this would not be true if the segregated streams where arranged in two horizontal stripes instead of the vertical arrangement expressed by Eq. (5). Panels B and C of Figure 15 show the spatial structure of the real, and imaginary part of the third (complex-valued) eigenfunction, respectively, that verify the symmetry relation $X(\rho, \zeta) = X(\rho, 1-\zeta)$.

This example shows how the first few eigenvalues-eigenfunctions of the spectrum can provide a characterization of the mixing process that is not constrained to a specific choice of the inlet condition, but depends only on the interaction between convective mixing and molecular transport.

Next, we show how the identification of the dominant eigenvalue for an assigned inlet profile can provide a mean for predicting the mixing length and the mixing time. Figure 16 shows the behavior of the mixing length N^{mix} (Panel A) and of the dimensionless mixing time $\tau^{\text{mix}} = N^{\text{mix}}/Re$ (Panel B) for the segregated inlet of Eq. (5) associated with 99% mixing vs the *Sc* number (indicated by the symbols N_{99}^{mix} and τ_{99}^{mix}, respectively). Note that mixing time is here defined by dividing the mixing length (expressed as number of mixer units, *N*) by the Reynolds number, which is proportional to the flowrate. The mixing length increases monotonically with *Sc*, but, for the reason explained in the previous Section when discussing mixing efficiency at fixed *Sc* conditions, its behavior is non- monotonic with respect to *De*. The mixing performance becomes instead monotonically increasing with the Dean number when the comparison between different flow conditions is made in terms of mixing time. In this case, at *Sc* values that are typical for ordinary liquid mixtures, the improvement of efficiency from, e.g., $De = 10$ to $De = 100$ is such as to lower the mixing time by more than a decade. Also note that for all the flow conditions considered, the behavior of τ_{99}^{mix} vs *Sc* is closer to a power-law dependence than to the logarithmic behavior that that is typically assumed for globally chaotic closed flows. [18]

The prediction of mixing length based on the dominant eigenvalue can be based upon the assumption that only the dominant eigenvalue contributes to the variance decay (i.e., assuming that the higher order contributions decay much faster then the dominant eigenmode),

$$\sigma(\Theta) = \sigma(0)e^{-\Lambda_d \Theta} = e^{-\Lambda_d 3\pi N} \Rightarrow N^{\text{mix}}(\overline{\sigma}) = \frac{1}{3\pi\Lambda_d}\log\left(\frac{1}{\overline{\sigma}}\right), \tag{26}$$

where $\overline{\sigma}$ is the degree of mixedness sought. Figure 17 shows the prediction of dimensionless mixing length for the inlet feed

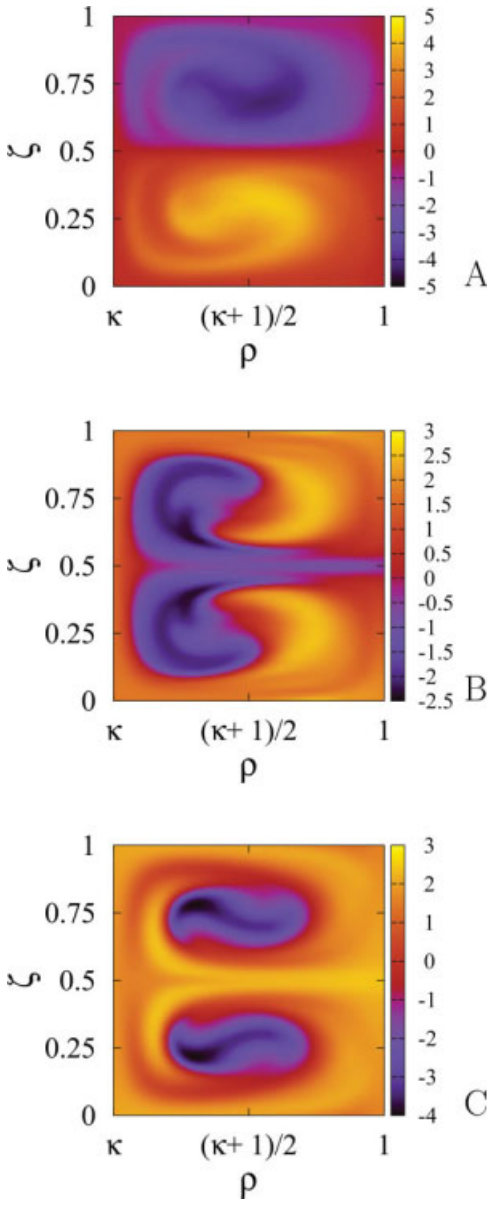

Figure 15. Spatial structure of the eigenfunctions of the Floquet operator at *De* = 50 and *Pe* = 10^5.

Panel **A**, first eigenfunction; Panel **B** and **C**, real part and imaginary part of the third eigenfunction. [Color figure can be viewed in the online issue, which is available at www.interscience.wiley.com.]

of Eq. (5) based on the second and on the third eigenvalue at different values of $\overline{\sigma}$, compared with the actual variance decay. At $De = 50$ (Figure 17A), the prediction agrees fairly accurately with the actual mixing length. At $De = 100$, the eigenvalue-based prediction tends to overestimated slightly the mixing length and becomes more and more accurate when increasing the degree of mixedness (i.e., when lowering $\overline{\sigma}$). This can be explained by the fact that when $\overline{\sigma}$ is decreased, the decay of variance associated with higher order eigenmodes becomes less and less important with respect to the overall decay accomplished when the the dominant exponential behavior has already settled in.

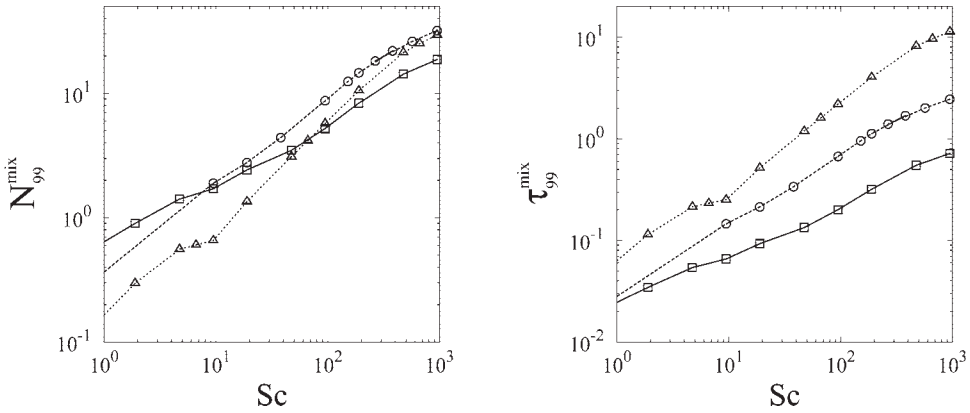

Figure 16. Dimensionless length, N_{99}^{mix}, and time, τ_{99}^{mix}, to reach 99% mixing at different values of *De*.

Continuous line and (□) symbols: $De = 100$. Dashed line and (○) symbols: $De = 50$. Dotted line and (◁) symbols: $De = 10$.

Concluding Remarks

In this article, we propose a new approach for quantifying mixing efficiency downstream an inflow–outflow mixer operating at steady state in the laminar regime. The approach stems from two assumptions that are verified by the vast majority of static mixers, be them operating at micro- or ordinary lengthscale, namely, (i) the spatially periodic structure of the flow, which makes it possible to single out a device unit (defined as the smallest spatial period of the flow), and (ii) the possibility of neglecting diffusion in the main streamwise direction, which is made possible by the large aspect ratio and by the large values of the Peclet number that characterize the geometry and operating conditions of typical mixing devices. Based on these assumptions, a Floquet operator, $\mathcal{F}$ mapping the scalar profile at the entrance of a generic unit into the profile at the unit exit can be defined. Because of spatially periodic structure of the flow, the characterization of mixing downstream the device at the exit of the n-th unit can be obtained through the repeated (n-fold) application of $\mathcal{F}$. The first few eigenvalues of the Floquet operator, ordered decreasingly with respect to their absolute value, provide an objective measure of the interaction between convective and molecular transport, where objective means that the spectral assessment of mixing efficiency is not dependent on the specific choice of the inlet profile. If the performance of a prescribed feeding condition is sought, then the decay of scalar variance far enough from the device entrance is described by the dominant eigenvalue associated with the inlet profile, which corresponds to the first nonzero coefficient of expansion of that profile in terms of the eigenfunctions of $\mathcal{F}$. The dominant eigenvalue can therefore depend upon symmetry properties of the scalar profile at the device entrance and/or of the eigenfunctions associated with the first eigenvalues of the ordered sequence.

We show that the spectral assessment of mixing efficiency overcomes the shortcomings of kinematics-based descriptions or of empirical indexes such as the mixing time. Specifically, even if seemingly similar to the kinematic approach (which is also based on the existence of a spatially periodic flow structure), the Floquet operator approach provides an intrinsically different description of the mixing process in that the interplay between convection and diffusion is here taken into explicit account. Once the spectral structure is known, the empirical indexes associated with a specific experiment can be predicted with good accuracy.

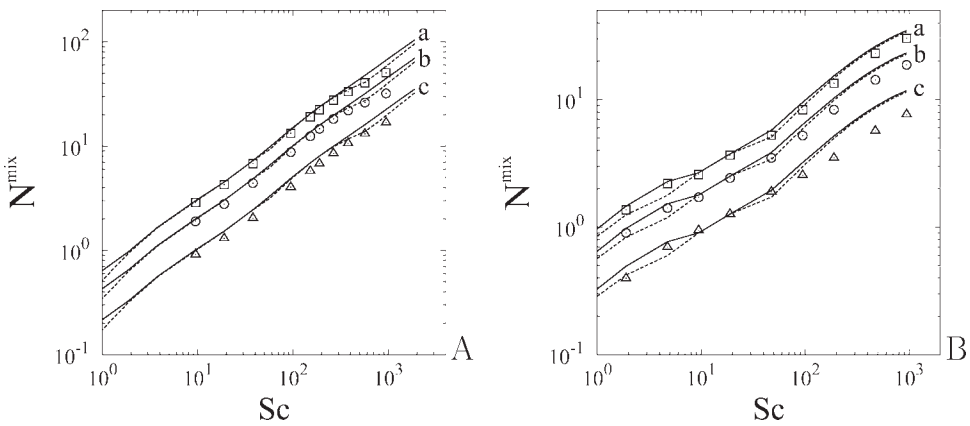

Figure 17. Dimensionless length to achieve different degrees of mixedness.

(◁), 90% mixing; (○), 99% mixing; (□): 99.9% mixing. The continuous and dashed lines represent the prediction based on the first and second eigenvalue, respectively, for (a): 99.9% mixing; (b) 99% mixing; (c) 90% mixing. Panel A, $De = 50$. Panel B, $De = 100$.

From the computational standpoint, an approximation to $\mathcal{F}$ can be obtained by projecting the advection-diffusion problem within a single device unit onto a finite-dimensional basis of expansion of the cross sectional profile. In principle, any projection basis, i.e., localized or global, can be used. Stemming from the simple geometric structure of the case study of this article, we use a global projection basis (Fourier modes with Neumann boundary conditions), which is typically less prone to numerical diffusion. Also, the simple device geometry allows us to compute a semi-analytical approximation to $\mathcal{F}$ by assuming a piecewise-constant structure of the velocity field along the device axis.

It is also worth remarking that the definition of a Floquet operator permits to analyze mixing in a device composed of an arbitrary long device, on the basis of the solution of the advection-diffusion problem in a single device unit. This makes it possible to investigate mixing in a device composed of several units, a problem that is computationally unfeasible if a direct solution in the entire mixing domain is pursued.

In closing, we want to point out that while the computational approach used for obtaining a representation of $\mathcal{F}$ in the S-shaped micromixer is to some extent specifically tailored to the simple device geometry of the case study analyzed in this article, the Floquet operator approach can be pursued even in more complex geometric architectures. One way to approach the computation could be as follows. Once the spatially periodic unit has been identified, and the basis of functions for expanding the cross sectional profile have been defined, the matrix representing the action of $\mathcal{F}$ can be constructed ''by columns'' by solving the advection-diffusion problem within the periodic unit for each of the basis function. Clearly, in the presence of geometrically complex boundaries (such as, e.g., the split-and-recombine mixer), the solution of each advection-diffusion problem must be obtained through localized approaches such as finite-volume or finite-element methods. In this case, the fact that devices with complex architectures generally operate at very small value of Re (of order unity or below) makes the problem of numerical diffusion less severe in that the Pe value associated with a typical liquid mixing problem is considerably lower than those associated with the same Sc value in the present case study.

Literature Cited

1. Aref H. The development of chaotic advection. *Phys Fluids*. 2002;14:1315–1325.
2. Vilkner T, Janasek D, Manz A. Micro total analysis systems. Recent developments. *Anal Chem*. 2004;76:3373–3386.
3. Squires TM, Quake SR. Microfluidics: Fluid physics at the nanoliter scale. *Rev Mod Phys*. 2005;77:977–1026.
4. Nguyen NT, Wu Z. Micromixers–a review. *J Micromech Microeng*. 2005;15:R1–R16.
5. Schönfeld F, Hardt S. Simulation of helical flows in microchannels. *AIChE J*. 2004;50:771–778.
6. MacInnes JM, Vikhansky A, Allen RWK. Numerical characterisation of folding flow microchannel mixers. *Chem Eng Sci*. 2007; 62:2718–2727.
7. Chen H, Meiners JC. Topologic mixing on a microfluidic chip. *Appl Phys Lett*. 2004;84:2193–2195.
8. Boesinger C, Le Guer Y, Mory M. Experimental study of reactive chaotic flows in tubular reactors. *AIChE J*. 2005;51:2122–2132.
9. Yamaguchi Y, Takagi F, Yamashita K, Nakamura H, Maeda H, Sotowa K, Kusakabe K, Yamasaki Y, Morooka S. 3-d simulation and visualization of laminar flow in a microchannel with hair-pin curves. *AIChE J*. 2004;50:1530–1535.
10. Vikhansky A. Coarse-grained simulation of chaotic mixing in laminar flows. *Phys Rev E*. 2006;73:056707.
11. Szalai ES, Muzzio FJ. Fundamental approach to the design and optimization of static mixers. *AIChE J*. 2003;49:2687–2699.
12. Finn D, Cox SM, Byrne HM. Mixing measures for a two-dimensional chaotic Stokes flow. *SIAM J Appl Math*. 2004;48:129–155.
13. Cerbelli S, Alvarez MM, Muzzio FJ. Prediction and quantification of micromixing intensities in laminar flows. *AIChE J*. 2002;48:686–700.
14. Jiang F, Drese KS, Hardt S, Küpper M, Schönfeld F. Helical flows and chaotic mixing in curved microchannels. *AIChE J*. 2004; 50:2297–2305.
15. Szalai ES, Kukura J, Arratia PE, Muzzio FJ. Effect of hydrodynamics on reactive mixing in laminar flows. *AIChE J*. 2003;49:168–178.
16. Yang JT, Lin KW. Chaotic mixing of fluids in a planar serpentine channel. *Int J Heat Mass Transfer*. 2007;50:1269–1277.
17. Vanka SP, Luo G, Winkler CM. Numerical study of scalar mixing in curved channels at low Reynolds numbers. *AIChE J*. 2004;50: 2359–2368.
18. Gleeson JP. Transient micromixing: Examples of laminar and chaotic stirring. *Phys Fluids*. 2005;17:100614.
19. Gleeson JP, West J, Roche OM, Gelb A. Modelling annular micromixers. *SIAM J ApplMath* ;64:1294–1310.
20. Mondal RN, Kaga Y, Hyakutake T, Yanase S. Bifurcation diagram for two-dimensional steady flow and unsteady solutions in a curved square duct. *Fluid Dyn Res*. 2007;39:413–446.
21. Karniadakis G, Beskok A, Aluru N. *Microflows and Nanoflows. Fundamentals and Simulations*. New York: Springer-Science, 2005.
22. Cerbelli S, Vitacolonna V, Adrover A, Giona M. Eigenvalue-eigenfunction analysis of infinitely fast reactions and micromixing regimes in regular and chaotic bounded flow. *Chem Eng Sci*. 2004;59:2125–2144.
23. Cerbelli S, Garofalo F, Giona M. Steady-state performance of an infinitely fast reaction in a three-dimensional open Stokes flow. *Chem Eng Sci*. 2008;63:4396–4411.
24. Reed M, Simon B. *Methods of Modern Mathematical-Physics: I. Functional Analysis*. New York: Academic Press, 1980.
25. Toussaint V, Carriere P, Scott J, Gence JN. Spectral decay of passive a passive scalar in chaotic mixing. *Phys Fluids*. 2000;12:2834–2844.
26. Wonhas A. Vassilicos JC. Mixing in fully chaotic flows. *Phys Rev E*. 2002;66:051205.
27. Kim HJ, Beskok A. Quantification of chaotic strength and mixing in a microfluidic system. *J Micromech Microeng*. 2007;17:2197–2210.

Manuscript received Jan. 13, 2009, and revision received May 19, 2009.